MODELING LIQUID CRYSTAL MATERIALS AND PROCESSES IN BIOLOGICAL SYSTEMS

Alejandro D. Rey

Department of Chemical Engineering - McGill University

Center for Scientific Computing and Mathematical Modeling

University of Maryland, College Park

April 19, 2007

Liquid Crystalline Phases

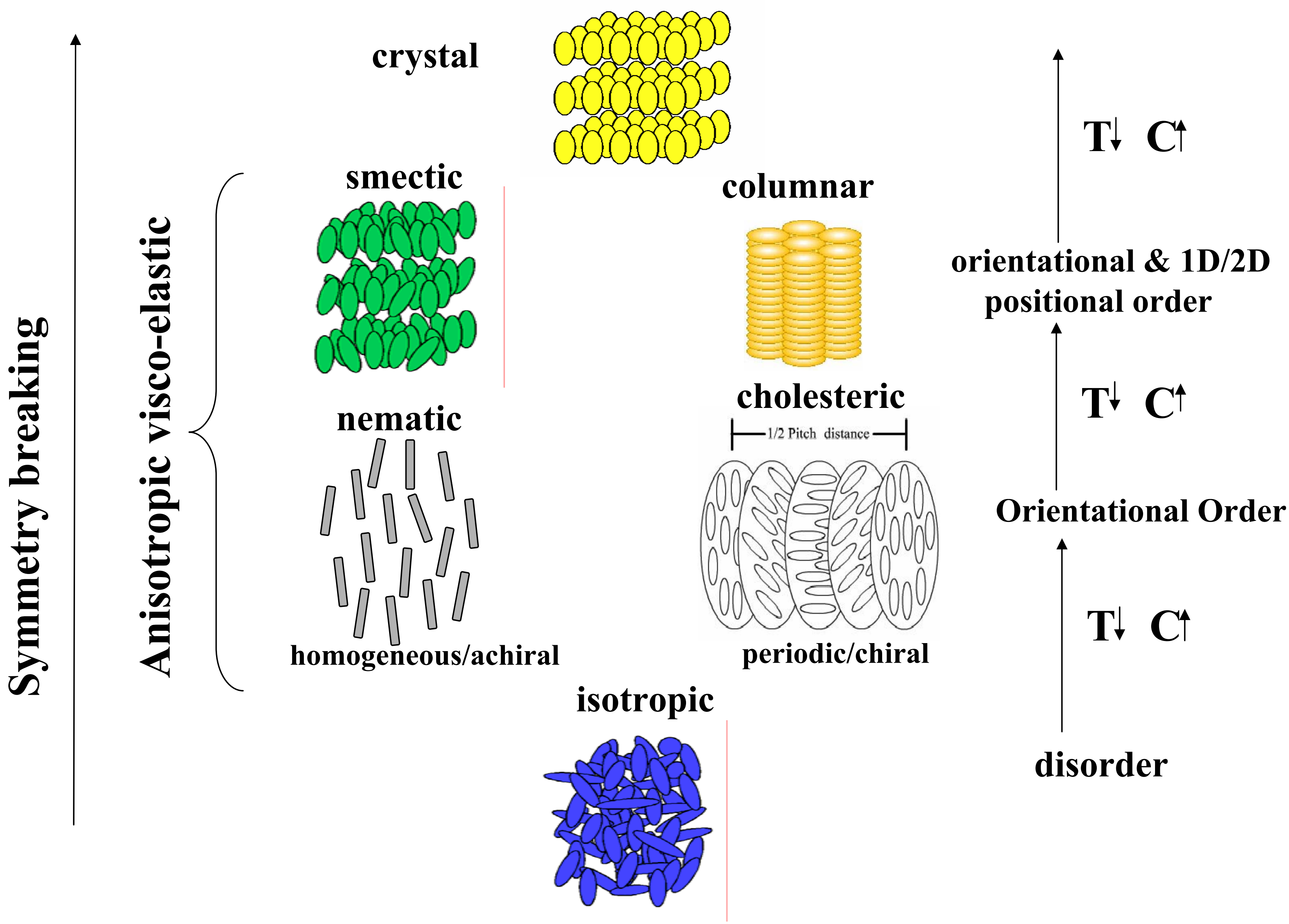

Modeling Biological Liquid Crystalline Materials and Processes

Precursors

Materials

Biological Polymer Processing

Device Modeling

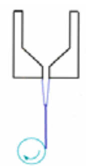

Structural BioLCs

Functional BioLCs

•Composites&Fibers& Films

•Lubricants&

Surfactants

Membranes

Sensors &

actuators

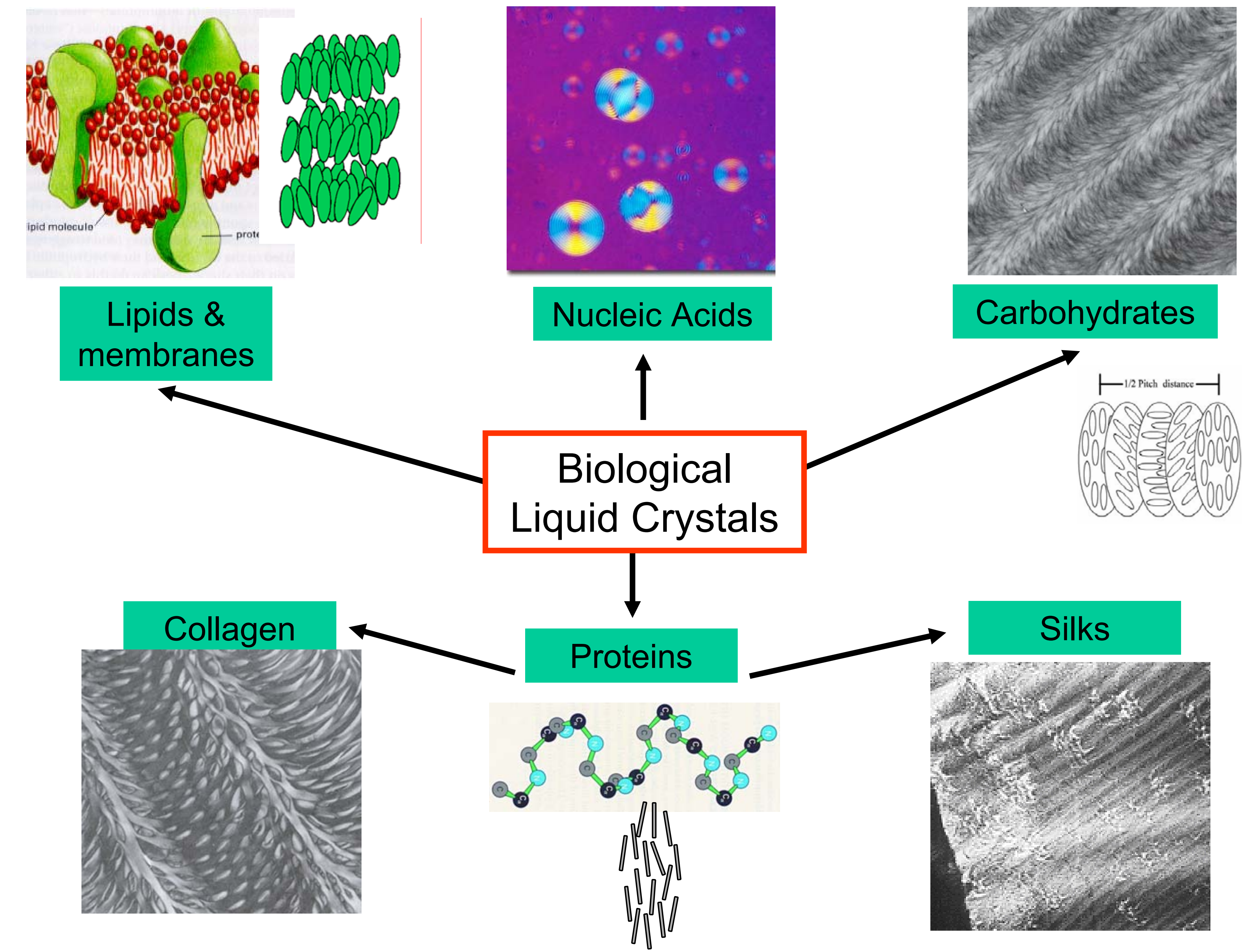

•T. Rizvi, Liquid crystalline biopolymers, J. Molecular Liquids 2003.

Liquid Crystal Biological Polymer Processing

systematic technology transfer from nature to engineering

Spider silk: Biospinning

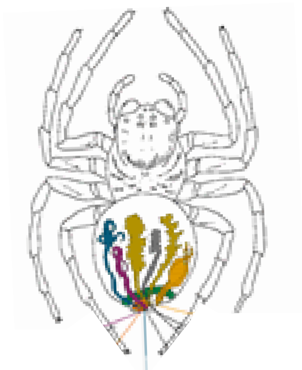

Fiber Spinning

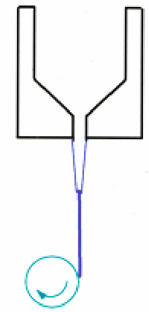

Mussel Byssus: biological reaction injection molding

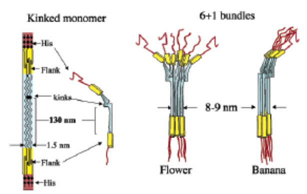

Figure 1. Proposed structure of the giant bent-core mesogens known as preCOLs that make up the bulk of mussel byssal threads. The block domain structure in 2D of a trimer (a); the bent-core analogue of a trimer (b); the proposed hexagonal (6+1) bundles of bent-core trimers in the flower and banana configurations. Amino to carboxy terminal orientation is left-to-right and top-to-bottom.

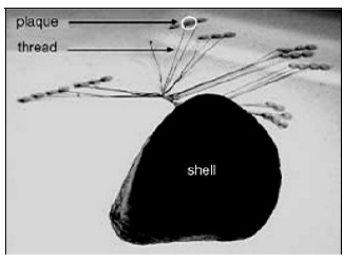

RIM

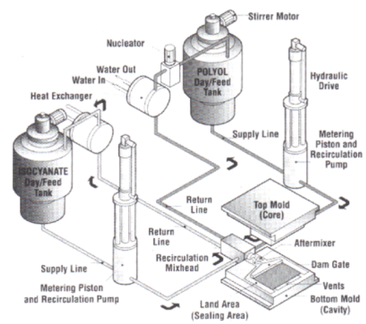

Chitin/collagen/keratin: biological composites

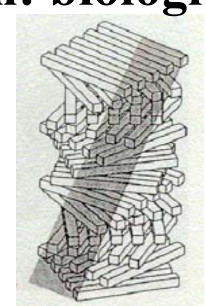

Composites

Fig. 13. ITV-braid-pultrusion: reel for core- and axial-yarns (1), braider with braiding yarns (2), preheating device (3), heated die (4), water cooling

Green engineering, sustainability, efficiency

American Journal of Botany 93(10): 1455–1465. 2006.

Onsager Self-Assembly Rigid Rod Model

V 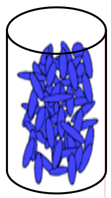

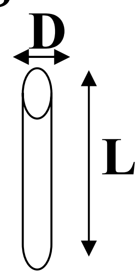

$$n\frac{\pi L^2 D/4}{4} = V \Rightarrow \boxed{\varphi\frac{L}{D} = 4}$$

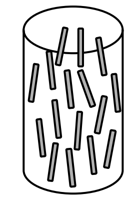

$$\Delta f/kT = \ln\left(\varphi\frac{L}{D}\right) + \underbrace{\int \Psi \ln(4\pi\Psi)\,d\Omega}_{\text{orientation}} + \underbrace{\frac{4}{\pi}\left(\varphi\frac{L}{D}\right)\iint \Psi(\Omega)\Psi(\Omega')\left|\sin\gamma\right| d\Omega d\Omega'}_{\text{excluded volume}}$$

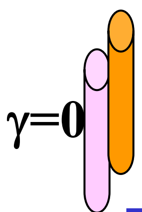

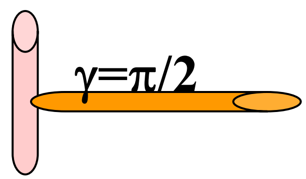

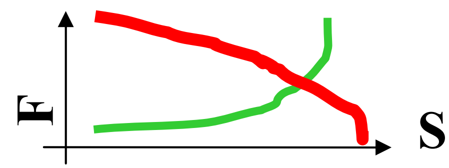

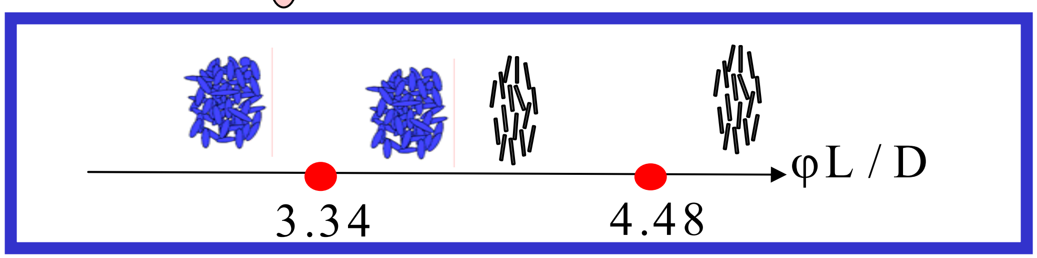

I/N transition in F-actin filaments

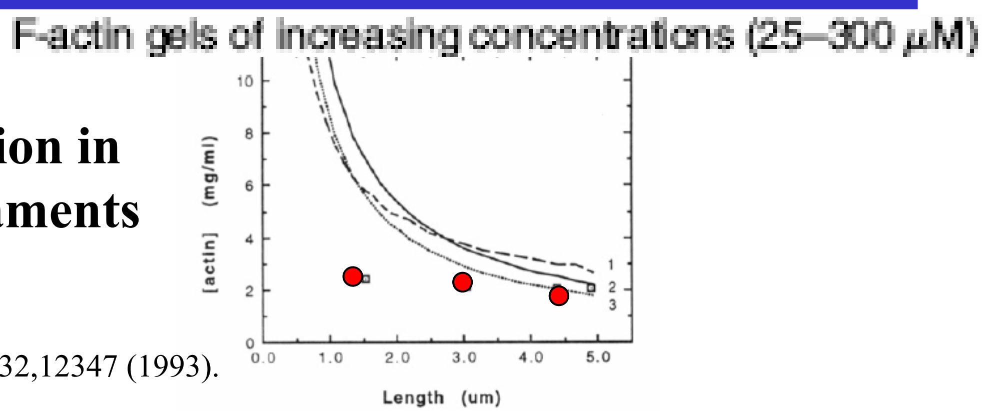

R.Furukawa et al , Biochemistry,32,12347 (1993).

Biophysical Journal Volume 89 July 2005 543–553

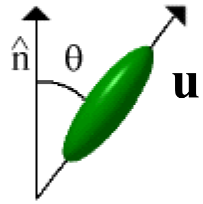

Maier-Saupe-Doi Rigid Rod Model

$$\Psi = e^{-\Phi/k_B T}/Z \qquad Z = \int e^{-\Phi/kT} d^2\mathbf{u}$$ **(partition function)**

Maier-Saupe-Doi Potential : $\Phi(\mathbf{u}) = -a_1 U \mathbf{Q} : \mathbf{uu}, U = \varphi L/D$

$$f_{MS} = U_{in} - TS = 3k_B TUS^2/4 - k_B T \ln Z$$

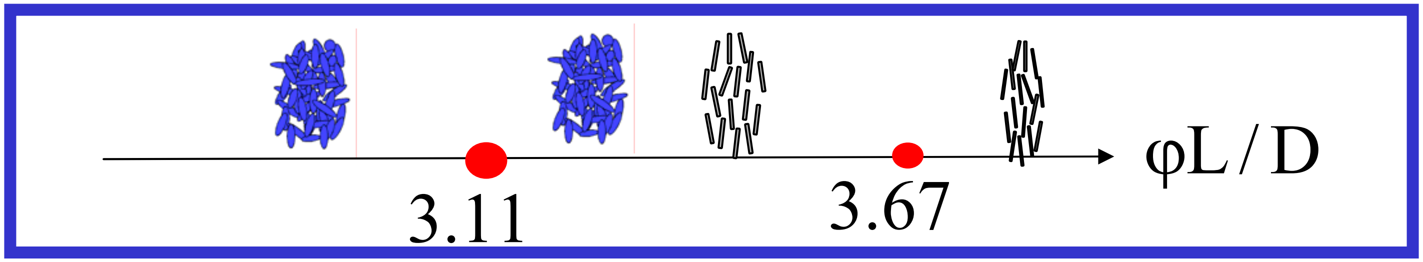

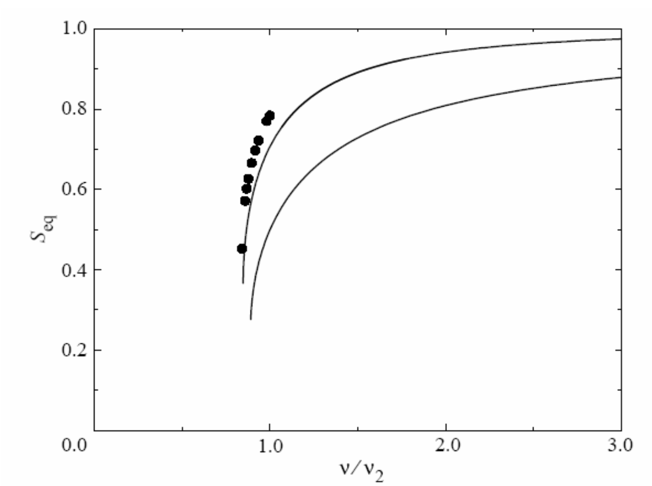

human melanocytes cells

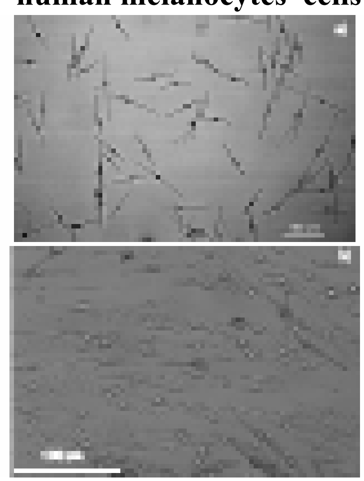

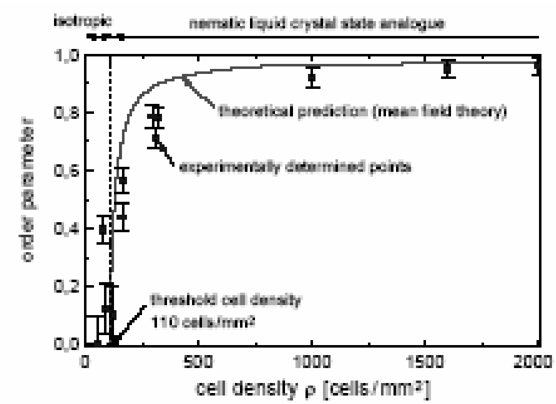

Fig. 8. Apolar order parameter, s, of melanocytes as a function of cell density. The dots are actual measurements. The line is a fit free prediction with $1/A_2 = 55$ cells/mm² [13].

Doi, 1981, Karlin, Ottinger (2000), R. Kemker et al, EPJ E, (2000)

INSTITUTE OF PHYSICS PUBLISHING JOURNAL OF PHYSICS: CONDENSED MATTER
J. Phys.: Condens. Matter 17 (2005) S3609–S3618 doi:10.1088/0953-8984/17/45/055

Kinetic pathways of the nematic–isotropic phase transition as studied by confocal microscopy on rod-like viruses

M Paul Lettinga[1], Kyongok Kang[1], Arnout Imhof[2], Didi Derks[2] and Jan K G Dhont[1]

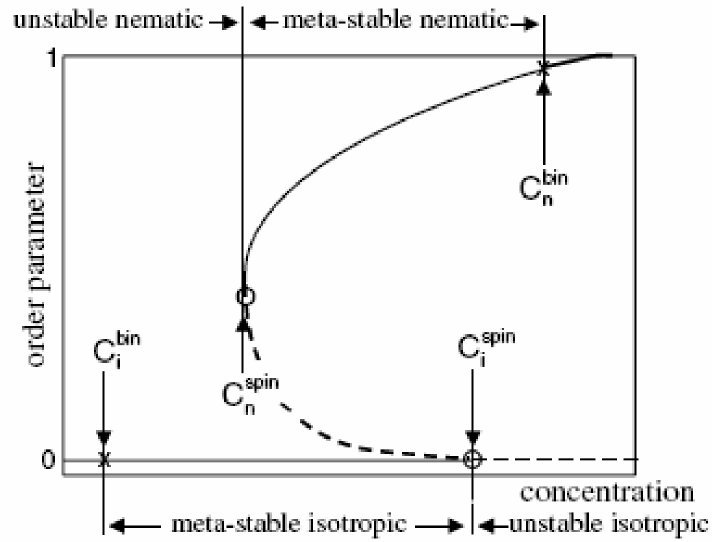

coexistence

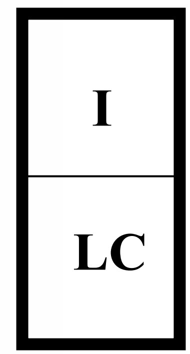

SD

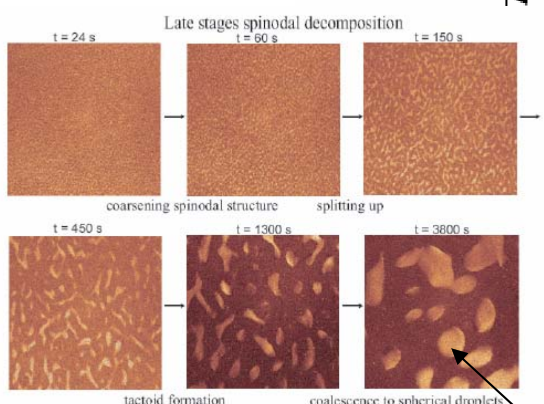

nematic

NG

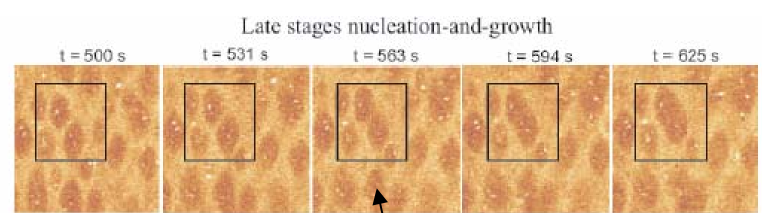

isotropic

Quadrupolar Order Parameter Q

Orientation n and Alignment S

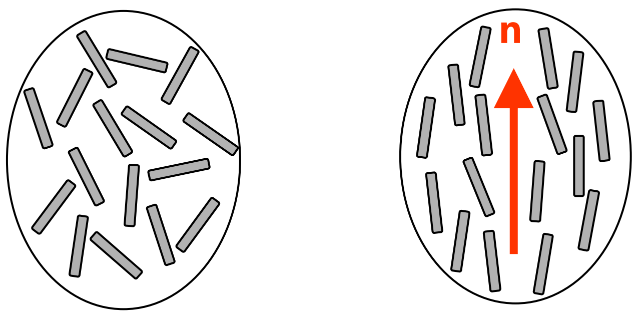

No alignment along n

S = 0

Intermediate alignment along n

S = 0.65

Perfect alignment along n

S = 1

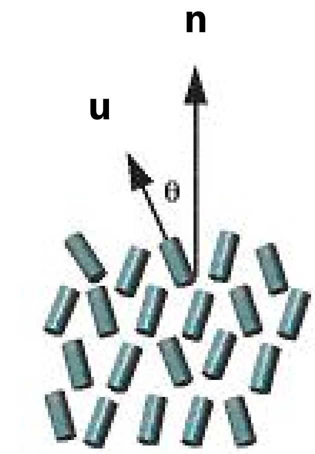

$$S = \frac{3}{2}\left\langle \cos^2\theta \right\rangle - \frac{1}{2}$$

Orientation & alignment Q

$$Q = S\left(nn - \frac{\delta}{3} \right)$$

Quadrupolar order parameter Q

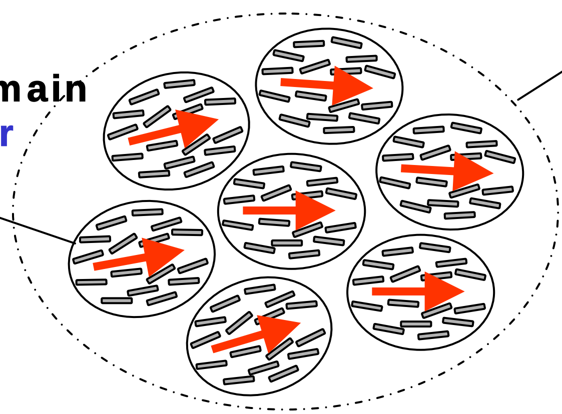

molecular domain
nanometer

Director field
micrometer

Macroscopic Chirality in Liquid Crystalline Phase

Cholesteric order=f (pitch, handedness, helix axis)

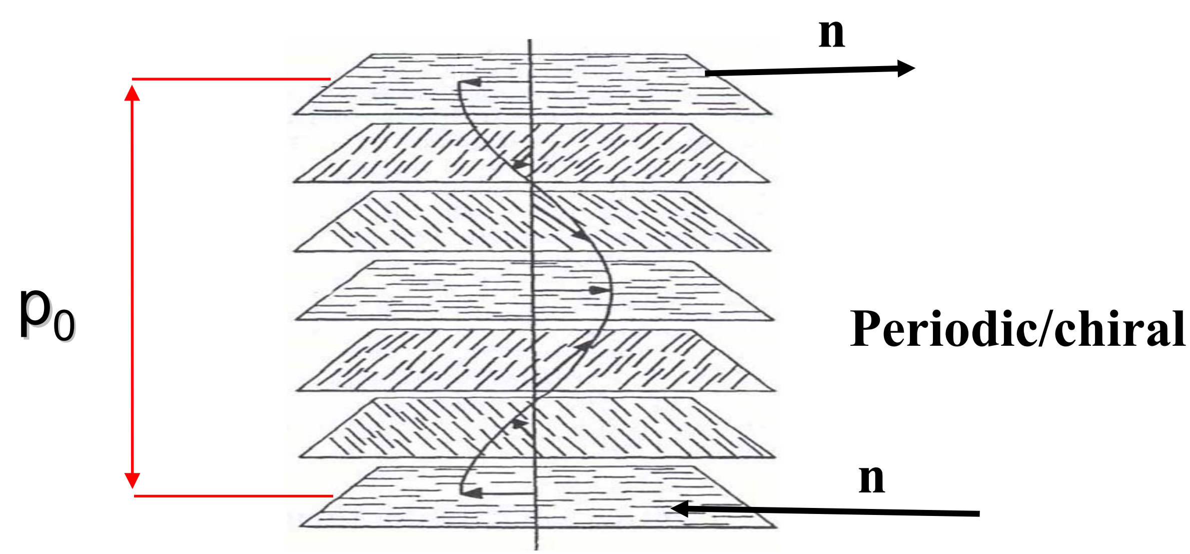

BIAXIAL QUADRUPOLAR ORDER PARAMETER

$$Q(z) = Q(z + p_o) = S\left(nn - \frac{\delta}{3}\right) + \frac{B}{3}(mm - ll)$$

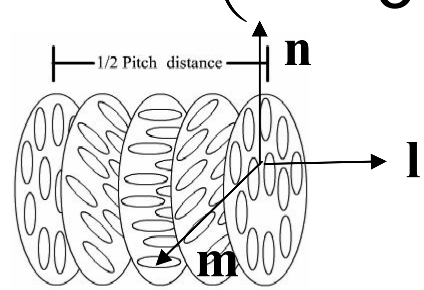

Chiral Nematics: Rules and Regulations

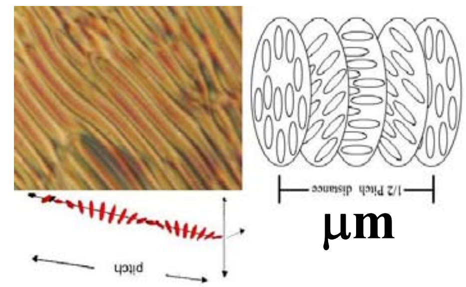

1. Molecular asymmetry;optical activity

$\mathrm{PBG}, L_p = 90\mathrm{nm}$ $\qquad$ $\mathrm{HPC}, L_p = 12\mathrm{nm}$

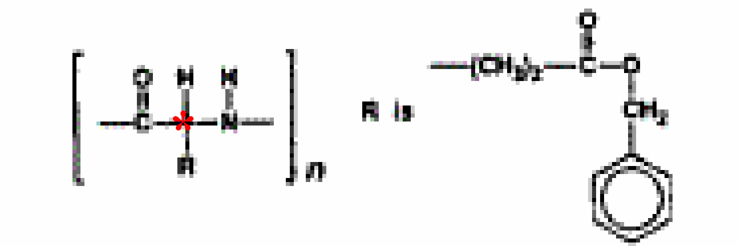

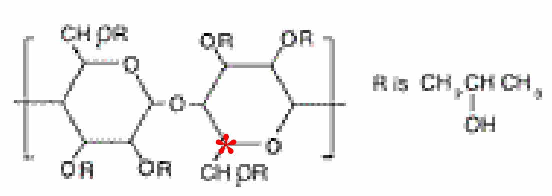

2. Some are formed by helical molecules

PBG **DNA** **collagen**

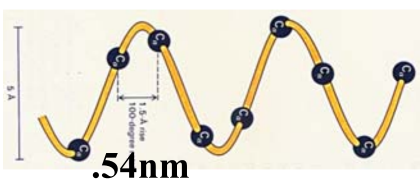

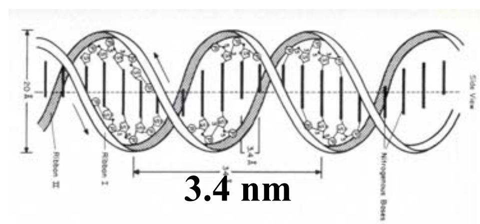

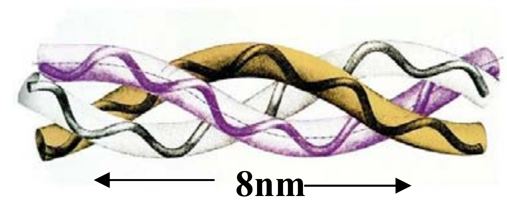

3. Geometric packing

$$\varphi L / D > 4 \pm \varepsilon$$

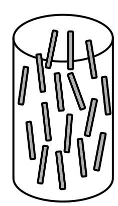

$$L_{DNA} = 50\mathrm{nm}, c_{DNA} \approx 100\mathrm{mg/ml}$$

A.C. Neville, Cambridge UP, 1993

Landau-deGennes Chiral Nematic Model

molecular chirality

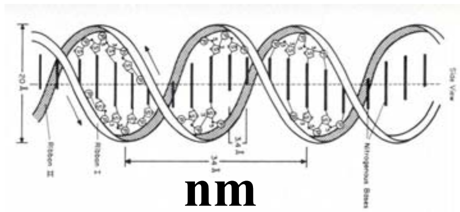

macroscopic chirality :h,R/L,P

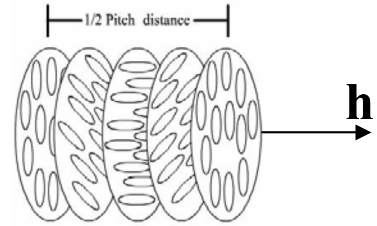

$$\Phi(\mathbf{u},\nabla\mathbf{u}) = -3/2 k_B T U \mathbf{Q} : \mathbf{u}\mathbf{u}^T$$

$$3/2 k_B T U \ell^2 \left(\left(\nabla \times \mathbf{Q} \right) + \left(\frac{4\pi}{p_0} \right) \mathbf{Q} \right) : \left(\nabla \times \mathbf{uu} + \left(\frac{4\pi}{p_0} \right) \mathbf{uu} \right)$$

orientation/excluded volume

$$f_h/cKT = \frac{1}{2}\left(1-\frac{U}{3}\right)\mathrm{tr}(Q^2) - \frac{U}{3}\mathrm{tr}(Q^3) + \frac{U}{4}[\mathrm{tr}(Q^2)]^2$$

chirality

$$f_g = \frac{L_2}{2}\left((\nabla \times Q) + \left(\frac{4\pi}{p_0}\right) Q \right)^2$$

Landau-deGennes Self-Assembly Model

$$S = \frac{1}{4} + \frac{3}{4}\sqrt{1 - \frac{4}{U}\left(\frac{2}{3} + \pi^2\left(\frac{\xi}{p_0}\right)^2\right)}$$

$$U_{IC} = 2.7\left[1 + 4\pi^2\left(\frac{\xi}{p_0}\right)^2\right]$$

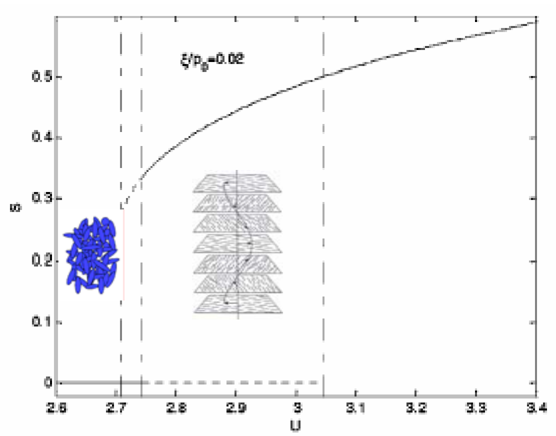

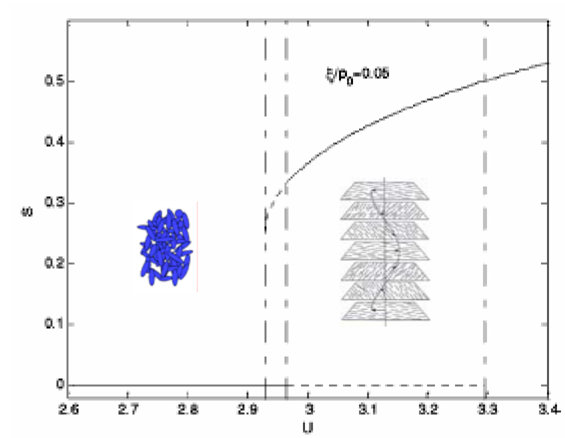

smaller pitch

higher packing

de Jeu and Longa, Phys.Reports (1980), Lhuiller&Rey JNNFM (2004), de luca and A.D. Rey PRE (2004)

Chiral Nematic: A Frustrated Mesophase

Short-fragment (146-bp) DNA , chicken erythrocytes

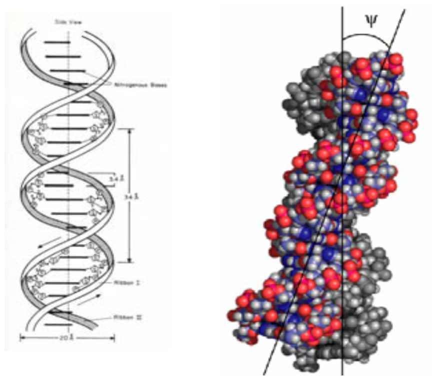

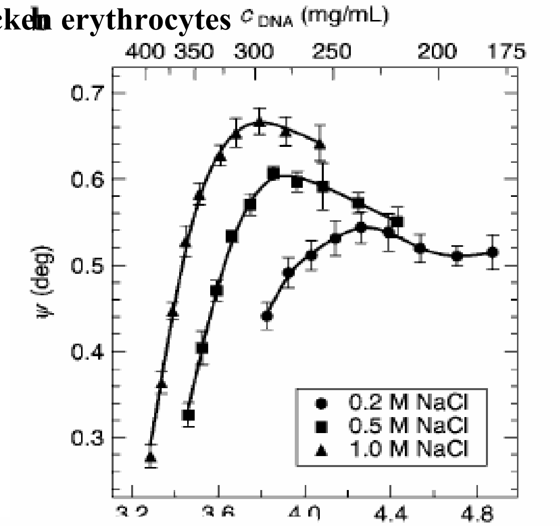

FIGURE 1 Illustration of the twist angle ψ between two DNA molecules. This angle, which is $<1°$, is directly related to the chiral interaction energy.

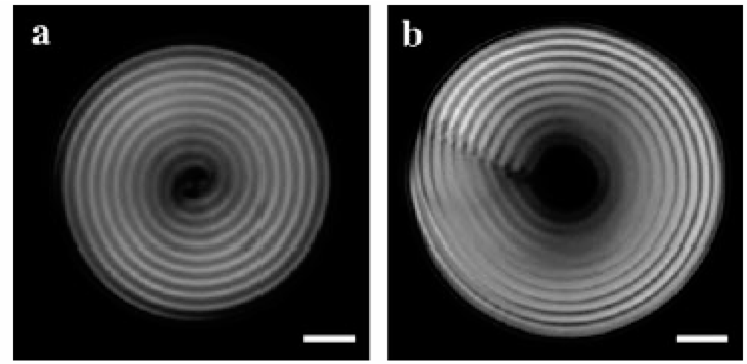

FIGURE 2 DNA cholesteric spherulites bathed in (*a*) 11 and (*b*) 17 wt % PEG 35,000 solutions (10:1 TE at pH 7.8, 0.5 M NaCl; scale bar = 5 μm). The distance between two striations represents the cholesteric pitch, which is ~2.7 μm for each of the spherulites shown. Both diametrical (*a*) and radial χ disclination (*b*) lines are observed in the spherulites.

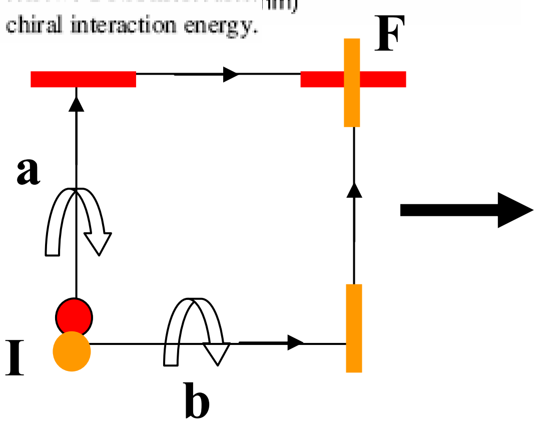

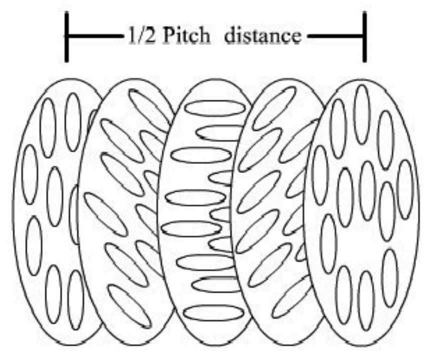

$$\delta n(F) = -\left(\frac{2\pi}{P_0}\right)^2 \left(n(I) \times (a \times b)\right)$$

P.Oswald and P. Pieranski, Nematics and Cholesteric LC, Taylor and Francis, 2005; C.B. Stanley et al, Biophysical Journal 89 (2005).

Landau-deGennes Chiral Self-Assembly Model

$$\gamma \frac{\partial Q}{\partial t} = -\left[\frac{\partial f}{\partial Q} - \nabla \cdot \frac{\partial f}{\partial \nabla Q} \right]^{[s]}$$

$$-\frac{\partial Q}{\partial t} = \left\{ (1-\frac{U}{3})Q - U(Q \cdot Q)^{[s]} + U\,\mathrm{tr}(Q^2)Q \right\}$$

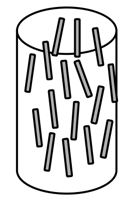

$$-\left(\frac{\xi}{h_0}\right)^2 \left(\nabla^2 Q - [\nabla \cdot (\nabla Q)^T]^{[s]} + \upsilon[\nabla(\nabla \cdot Q)]^{[s]}\right)$$

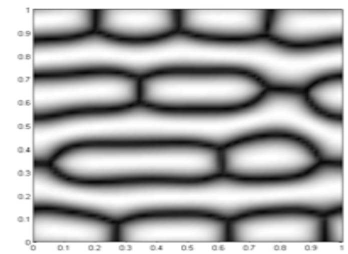

$$\left(\frac{\xi}{h_0}\right)\left(\frac{\xi}{p_0}\right)\left(-8\pi(\nabla \times Q)^{[s]}\right) + \left(\frac{\xi}{p_0}\right)^2 \left(-16\pi^2 Q\right)$$

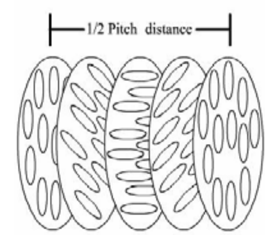

$p_0 \to \infty$

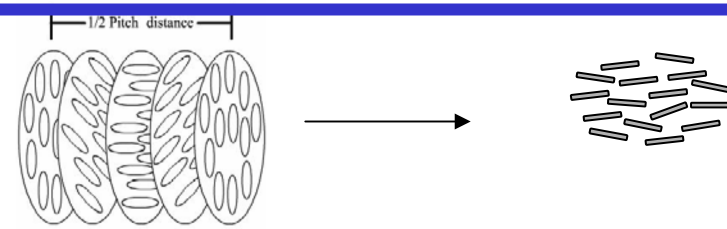

Modeling Biological Liquid Crystals

I. DNA solutions: textures and flows

Landau-deGennes, Leslie-Ericksen Nematodynamics

I. Biphasic Equilibrium: Tactoids

Liquid Crystal Laplace-Herring Equation

Main Task: Use modeling to recognize and characterize biological liquid crystal self-assembly

I.Packing helices into small volumes → condensed phases of DNA

Table 6. Sequence of the different liquid crystalline and crystalline phases with characteristic parameters determined for DNA in 0.25 M ammonium acetate buffer **140 base pairs, 50nm**

	isotropic	cholesteric	hexagonal 2D	hexagonal 3D	orthorhombic
C (mg/ml)	160	380		670	1055
		mean interhelix distance am: 49Å … 32 Å	interhelix distance aH: 31.5Å 29Å	23.7Å	lattice parameters: a = 24.09Å, b = 39.33 Å; a = 20.77Å, b = 29.72Å
			pitch of the DNA helix: 34.6Å		30.2Å

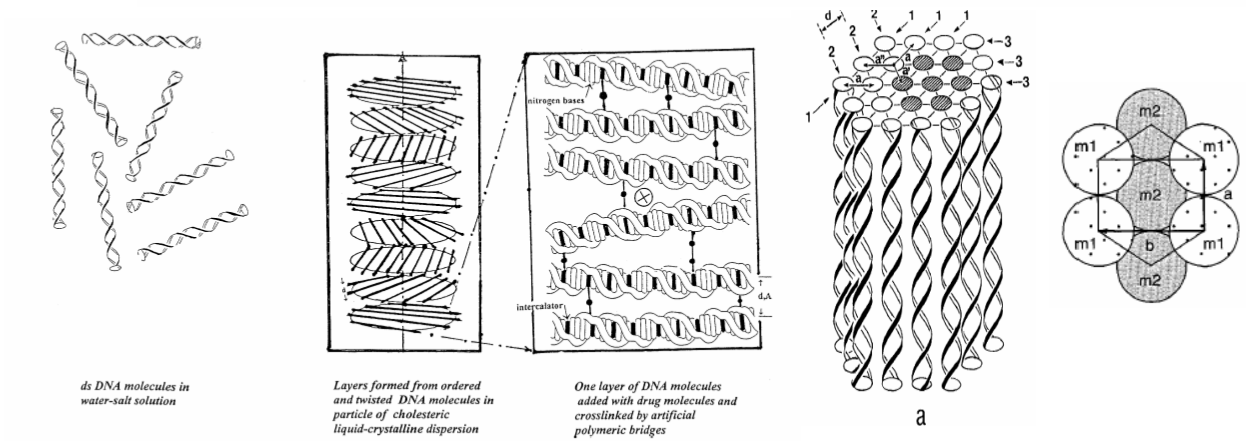

chirality

$$\left((\nabla\times Q)+\left(\frac{4\pi}{p_0}\right)Q\right)^2$$

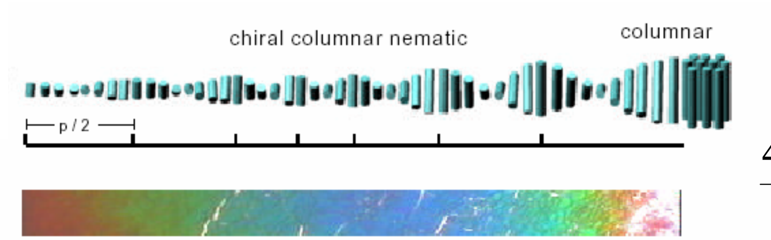

FIGURE 1 Model of the structural changes which could explain the variation of the pitch length with changing the concentration of the solvent in the chiral columnar phase.

excluded volume

$$\frac{4L\varphi}{\pi D}\iint f(\Omega)f(\Omega')|\sin\gamma|d\Omega d\Omega'$$

Livolant, Leforestier, Prog. Polym. Sci., 1996

Cholesteric Packing of DNA

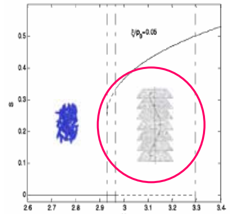

Textured/Polycrystal

Cryoelectron microscopy of stallion sperm: 80nm sections,2.7nm filaments, 30 filaments

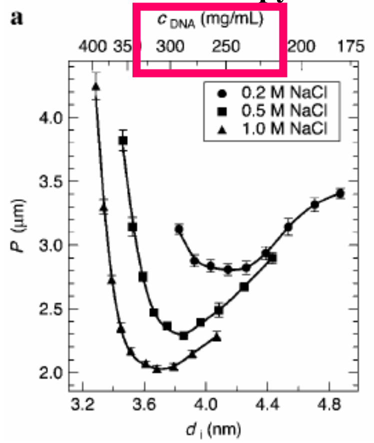

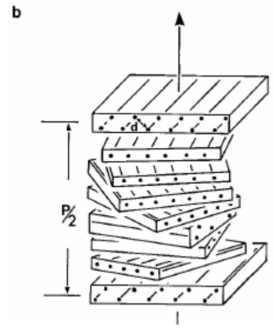

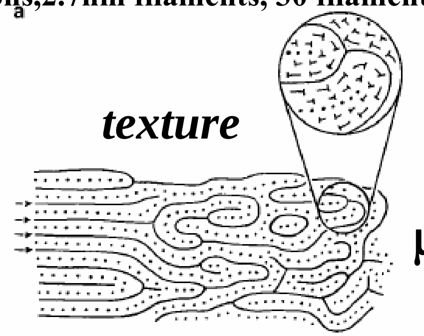

simulations

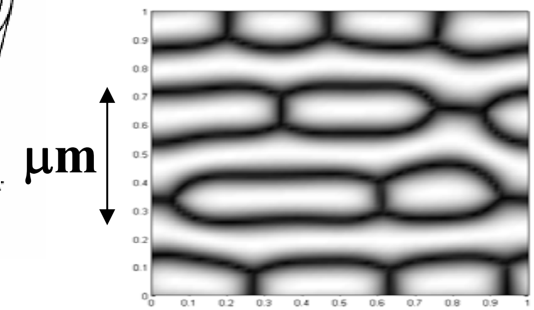

MonoCrystal

Cholesteric DNA in Dinoflagellates

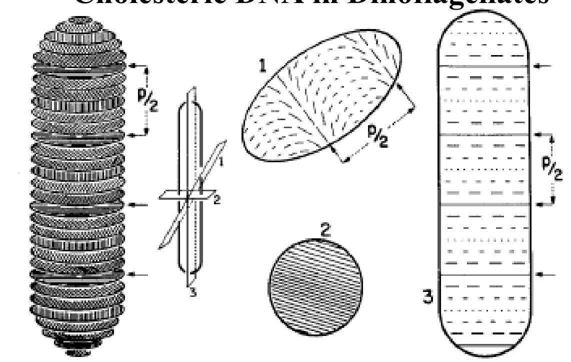

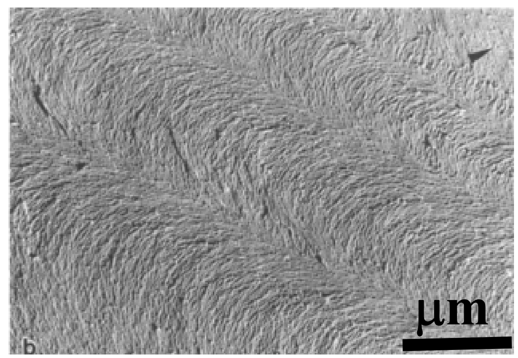

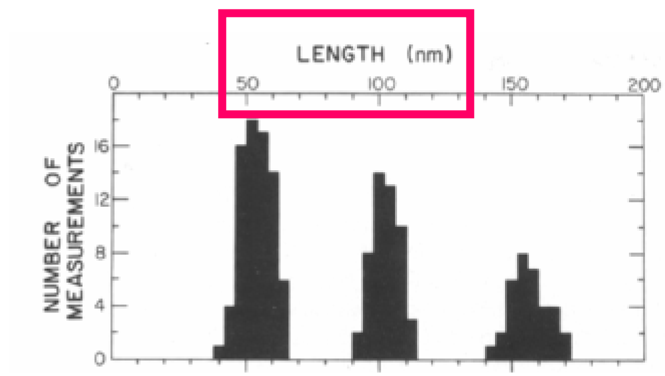

simulations

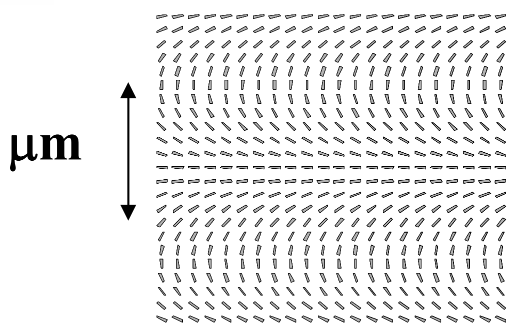

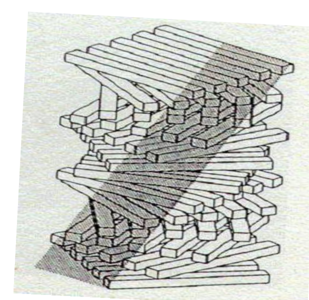

R.Rill et al, Chromosoma , 1989. Livolant, Leforestier, Prog. Polym. Sci., 1996 G.deLuca and A.D.Rey, EJP (2003

Fingerprinting: τ Disclination Lines in DNA Cholesteric Textures

non-singular | **singular**

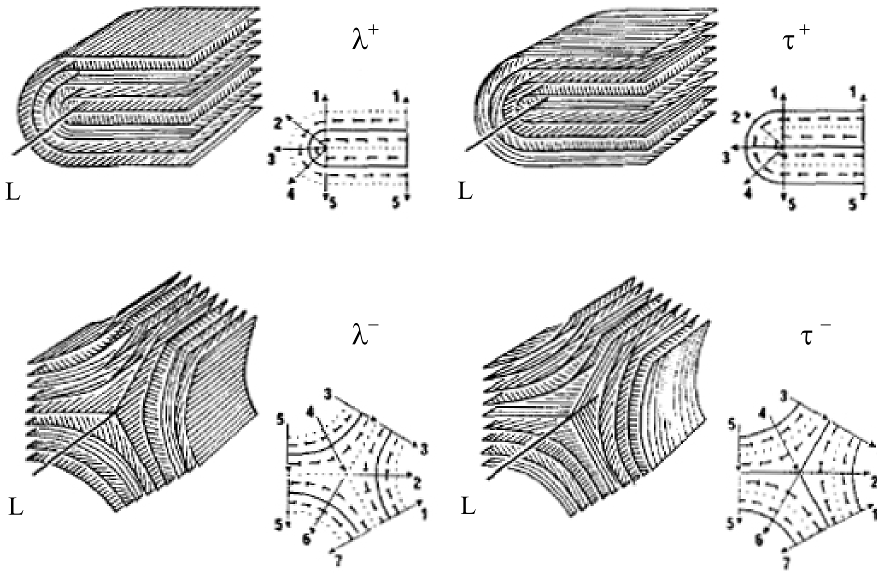

Defects and textures serve to identify LC phases using POM:

finger-print

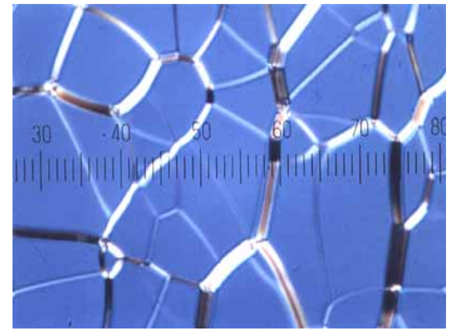

Grandjean

Ch DNA

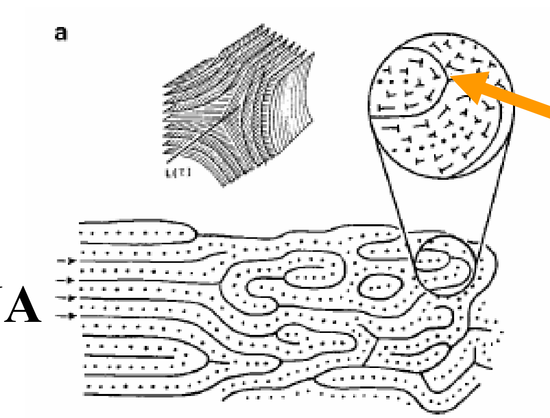

τ -texture simulations

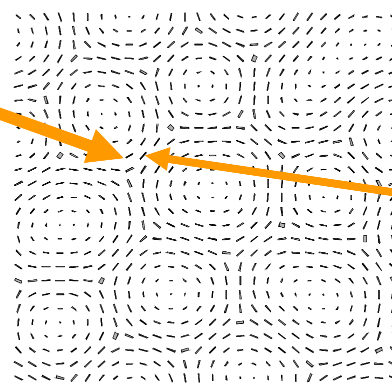

τ defect cores

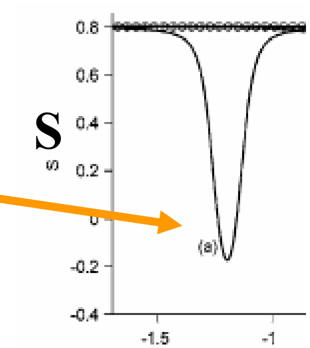

G.deLuca and A.D.Rey, EJP (2003), Livolant, Leforestier, Prog. Polym. Sci., 1996   deGennes and Prost (1991)

Liquid Crystallinity in Spreading DNA Drops

diluted solution of salmon sperm DNA under drying process

m=20mg

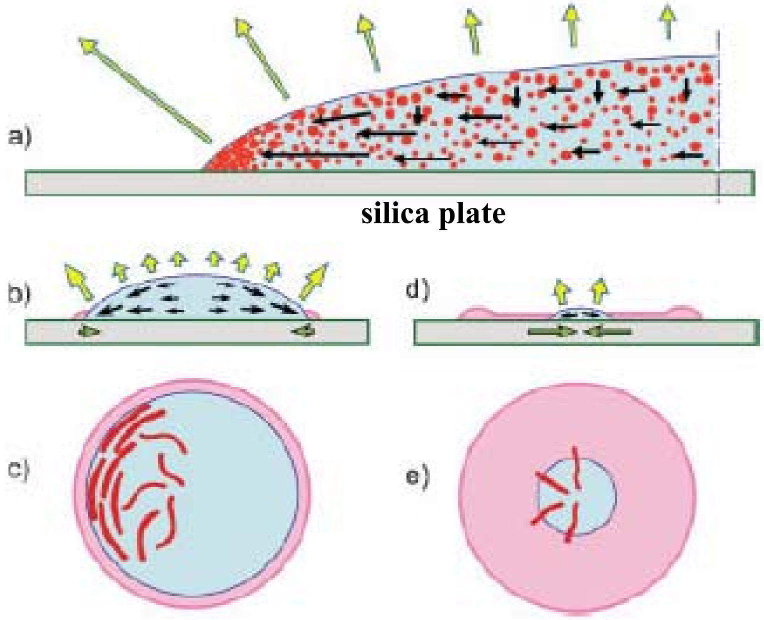

Before use, these DNA samples were redissolved in water or buffer solution by standing still for 2 weeks. To compare the pH dependence of this phenomenon, solutions at pH 3.0, 9.0, and 12.5 were prepared by the addition of phosphoric acid or aqueous sodium hydroxide to the original DNA solution, whose pH was 6.8. The concentrations of these DNA solutions were at first adjusted to 31 mg/ml, which is

Table I Molecular Weights of DNA Samples

DNA	Sonication (h)	M_{SEC}[a] (kbp)	M_w[b] (kbp)
SD-29	0	5.3	29
SD-23	0.2	4.2	23
SD-22	0.5	4.1	22
SD-9	3	1.8	8.8
SD-6	5	1.2	5.6
SD-1	10	0.26	1.4

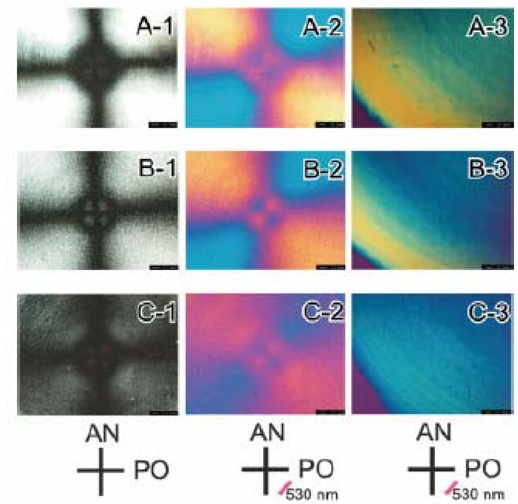

Leslie-Ericksen Nematodynamics Simulations

DNS Maxwell Eqns

extensional zone

shear zone

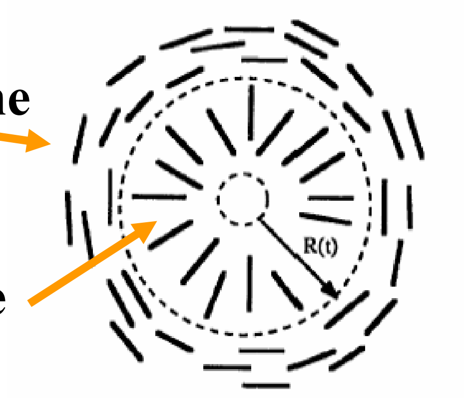

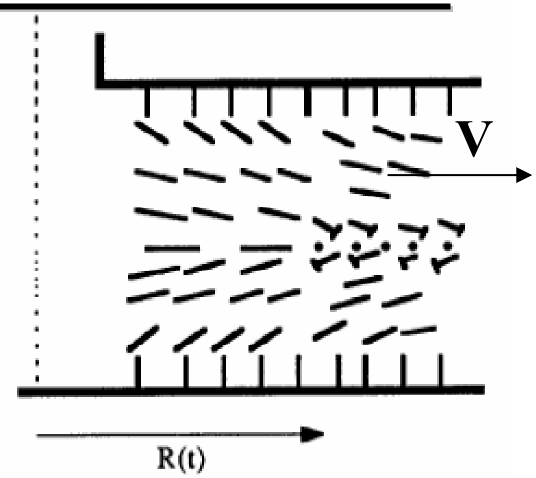

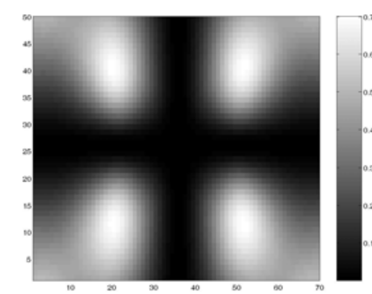

A.D. Rey, JOR (1991).

N.Morii et al

Biopolymers, Vol. 77, 163–172 (2005)

II. Looking at the I/LC Phase Boundary: Biological Tactoids

At coexistence bioLCs drops should be tactoids!

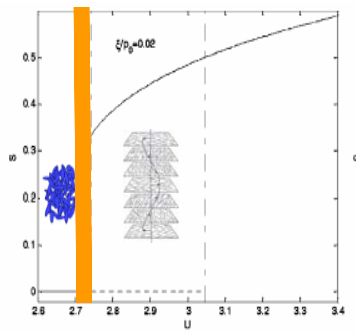

Helical Flagella

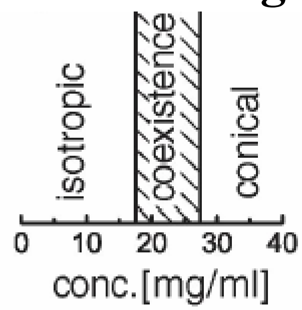

Salmonella typhimurium.

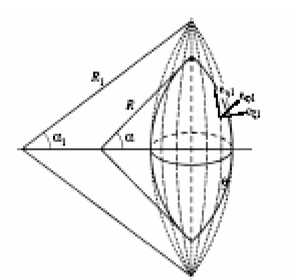

F-Actin

μm

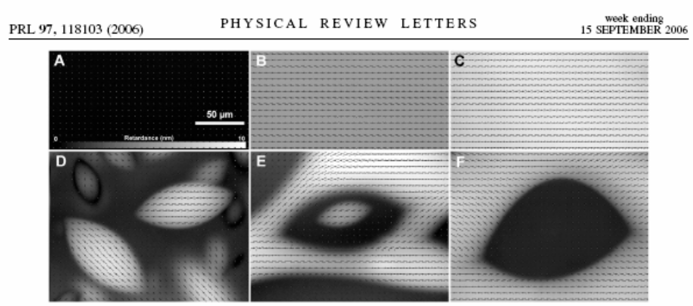

FIG. 1. Birefringence measurement of F-actin solutions at $l = 11\ \mu$m (a),(b),(c) and at $l = 1\ \mu$m (d),(e),(f). The 50 μm scale bar and the gray scale intensity bar, indicating retardance values from 0 to 10 nm, apply to all the images. The line segments represent the local direction and relative magnitude of filament alignment. (a),(b),(c) Representative samples are shown in the I phase, in the I-N transition region for long F-actin, and in the N phase, respectively. No discontinuity is detected in the transition region. (d),(e),(f) At $l = 1\ \mu$m and in the I-N transition region, F-actin phase separates into tactoidal droplets: N droplets in an I background (d), coexistence of N and I droplets (e), and an I droplet in a N background (f).

Amyloid fibrils

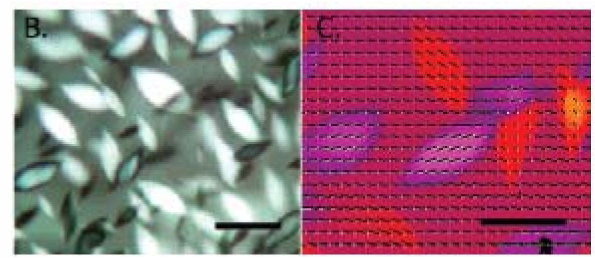

Tactoid simulations

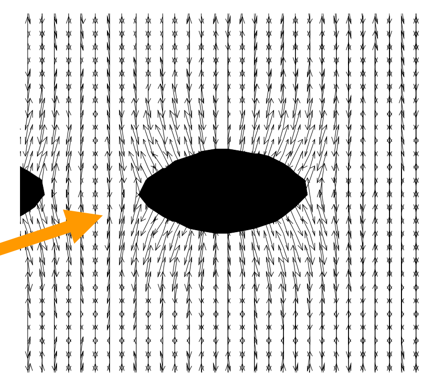

Liquid Crystal Laplace Equation

$$\Delta P = \underbrace{-\left(\nabla_s \cdot \mathbf{k}\right)\gamma_o}_{spherical} + \underbrace{W\left(-\nabla_s \mathbf{k} : \mathbf{nn} + \left(\nabla_s \cdot \mathbf{k}\right)\left(\mathbf{n} \cdot \mathbf{k}\right)^2\right)}_{non-spherical}$$

The shape yields interfacial and bulk elasticity moduli

A.D. Rey, JCP (2004), PRE(2004), S.Das and A.D. Rey MTS (06)

Modeling Biological Liquid Crystalline Materials and Processes

Precursors

Biological Polymer Processing

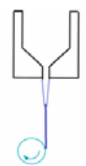

Structural BioLCs

- Composites: helicoids
- Fibers&Films : silk, cellulosics, collagen, chitin

Materials

Device Modeling

Functional BioLCs

- Lubricants: synovial fluids, mucus

  Surfactants: bile salts

Membranes

Sensors& actuators

Biological Fibrous Composites

“Nature uses Cholesteric Liquid Crystal Self-Assembly to produce High Performance Structural Composites”

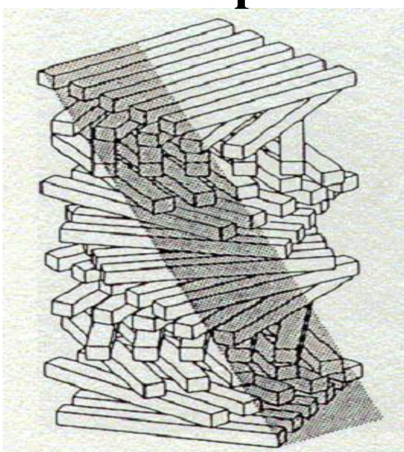

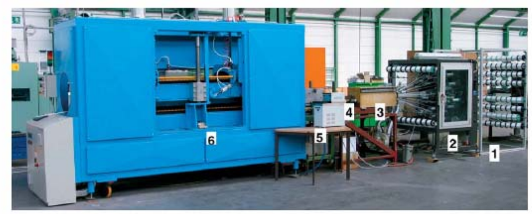

Fig. 13. ITV-braid-pultrusion: reel for core- and axial-yarns (1), braider with braiding yarns (2), preheating device (3), heated die (4), water cooling

Main Issues: How do they form? What controls the kinetics? Develop models that describe selection/evolution of fiber orientation.

Y. Bouligand, “Liquid crystal and their analogues in biological systems”, Solid State Physics, Academic Press, 1978
M.M. Giraud-Guille, “Twisted Liquid Crystalline Supramolecular Arrangements In Morphogenesis”, *International Review of Cytology*, 1996
A.C. Neville, “Biology of Fibrous Composites”, Cambridge University Press, 1993

Universal structural motif of fibrous biological materials

Cross-section of a crab carapace

chitin

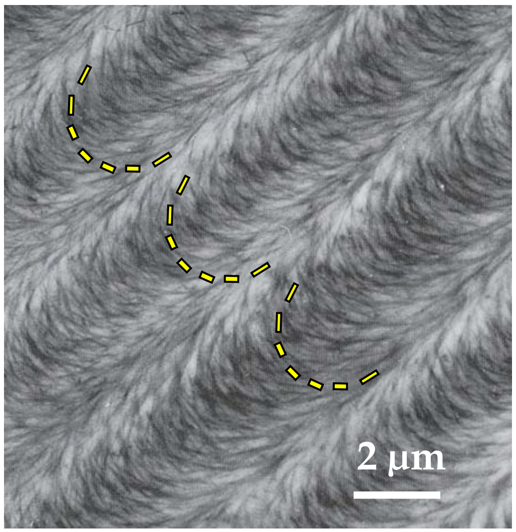

Cross-section of a human bone

collagen

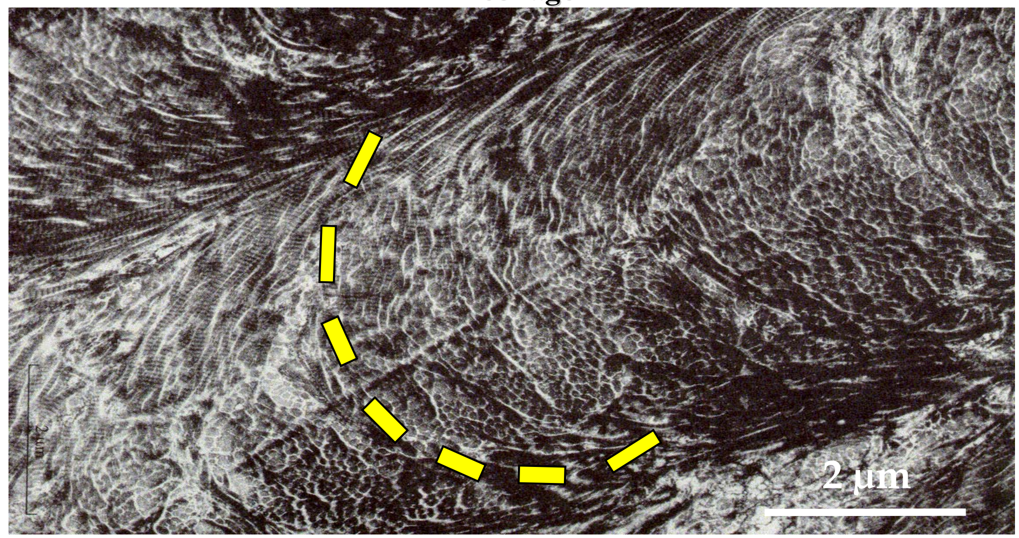

Cross-section of the stone cell of a pear

cellulose

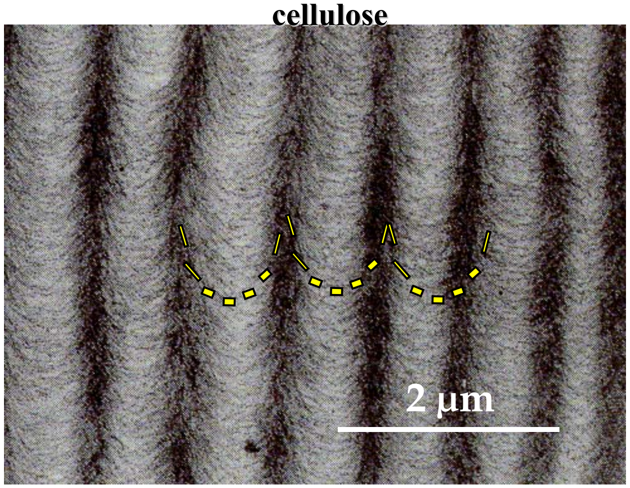

Cuticle of dragonfly

chitin

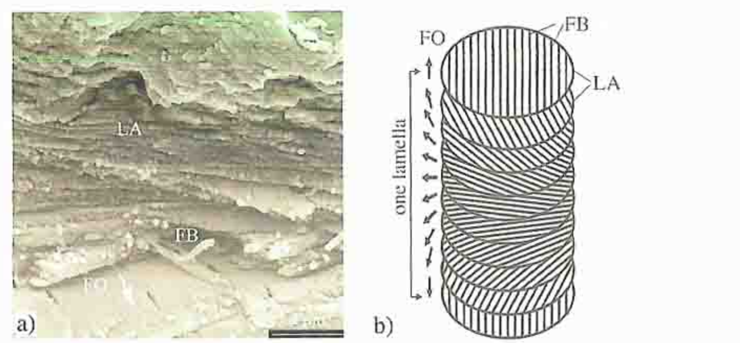

Fig. 4.3. Ultrastructural architecture of the procuticle. (**a**) Fractured cuticle of the rear surface of the head of the dragonfly *Sympetrum sanguineum*. (**b**) Schematic of the cuticle lamella. FB, fibers; FO, preferred orientation of the fibers; LA, layers of fibers.

A.C. Neville, "Biology of Fibrous Composites", Cambridge University

Helicoids: Plywood architecture with chiral nematic order

Normal cross-section

Fiber orientation

Oblique cross-section

Arced patterns

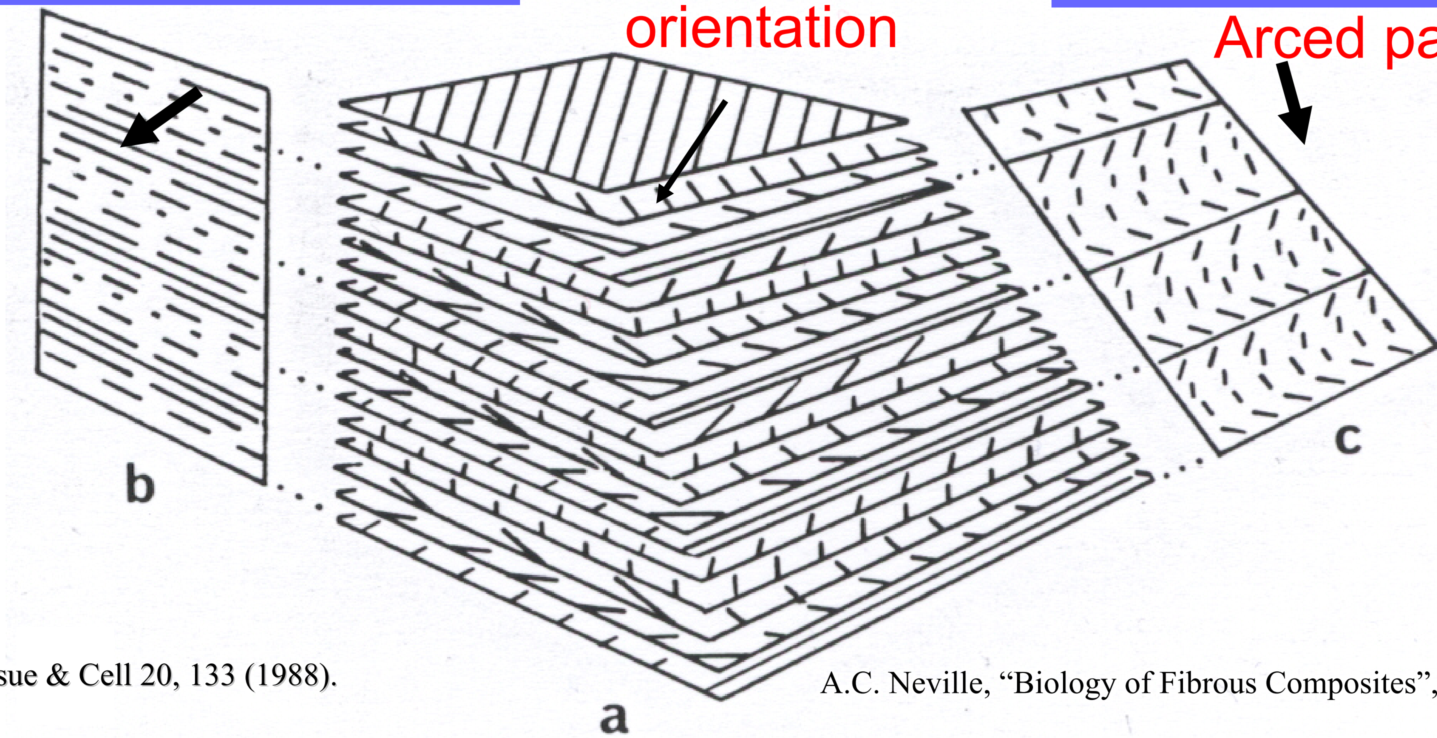

Neville,Tissue & Cell 20, 133 (1988).

A.C. Neville, “Biology of Fibrous Composites”, Cambridge University

Polydomain plywood

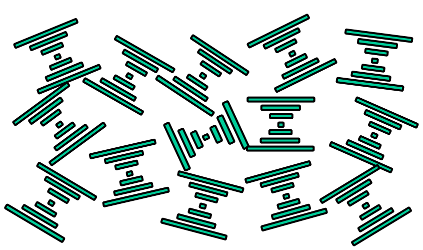

Without a constraining layer

Planar monodomain plywood

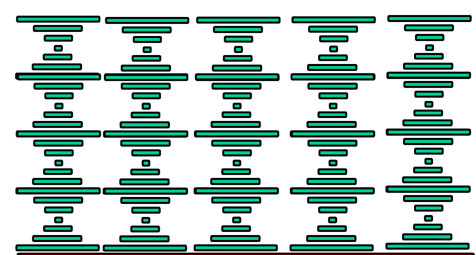

With a constraining layer

Kinetics of Composite Formation

Traveling Fronts

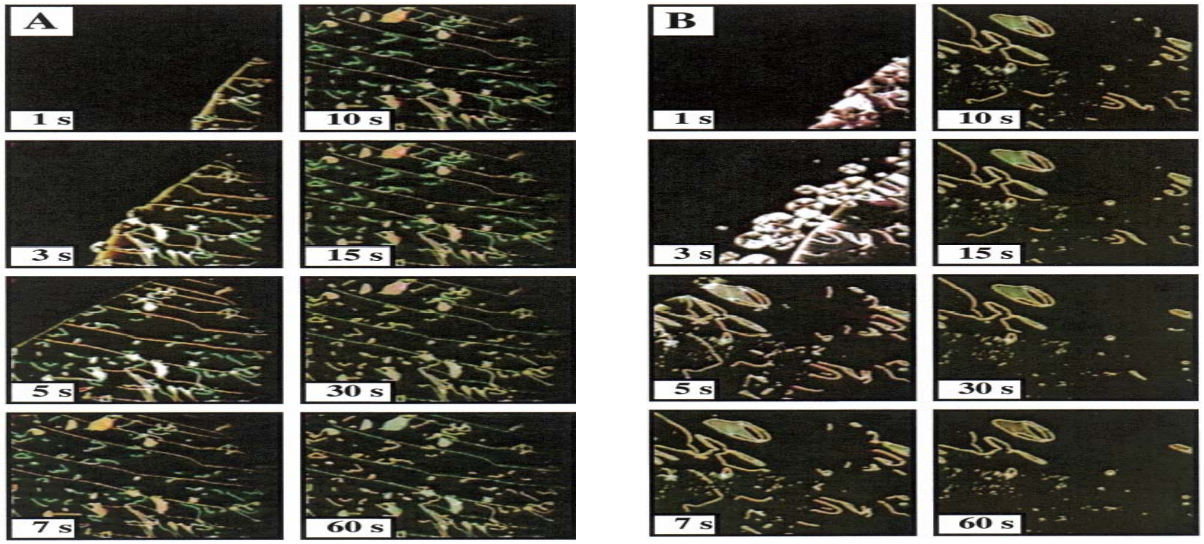

Static Solitons: Topological Defects

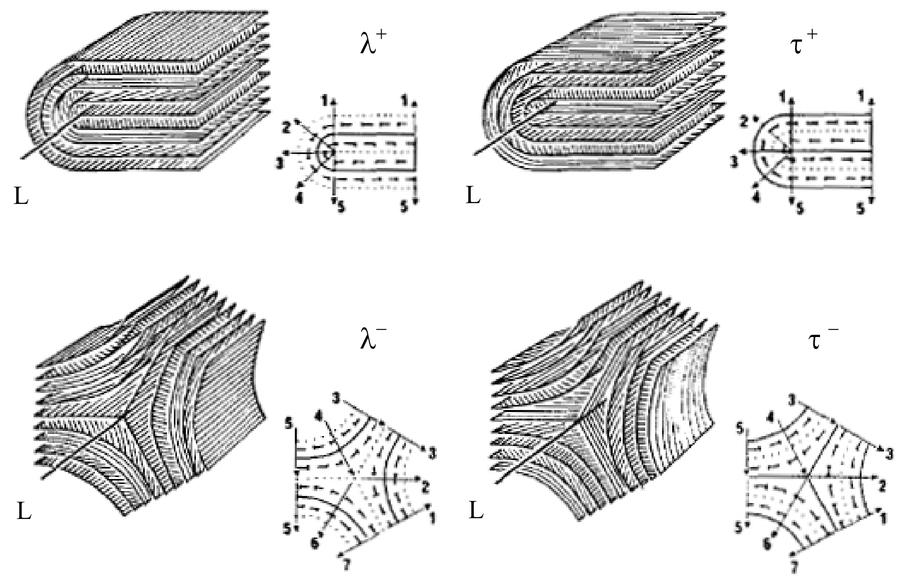

Skaife JJ, Abbott NL, (2001)
Langmuir, 17, 5595-5604.

Solitons and Traveling Fronts: Sink-Source-Saddle Connections

$$Q(z) = S\left(nn - \frac{\delta}{3}\right) + \frac{B}{3}(mm - ll)$$

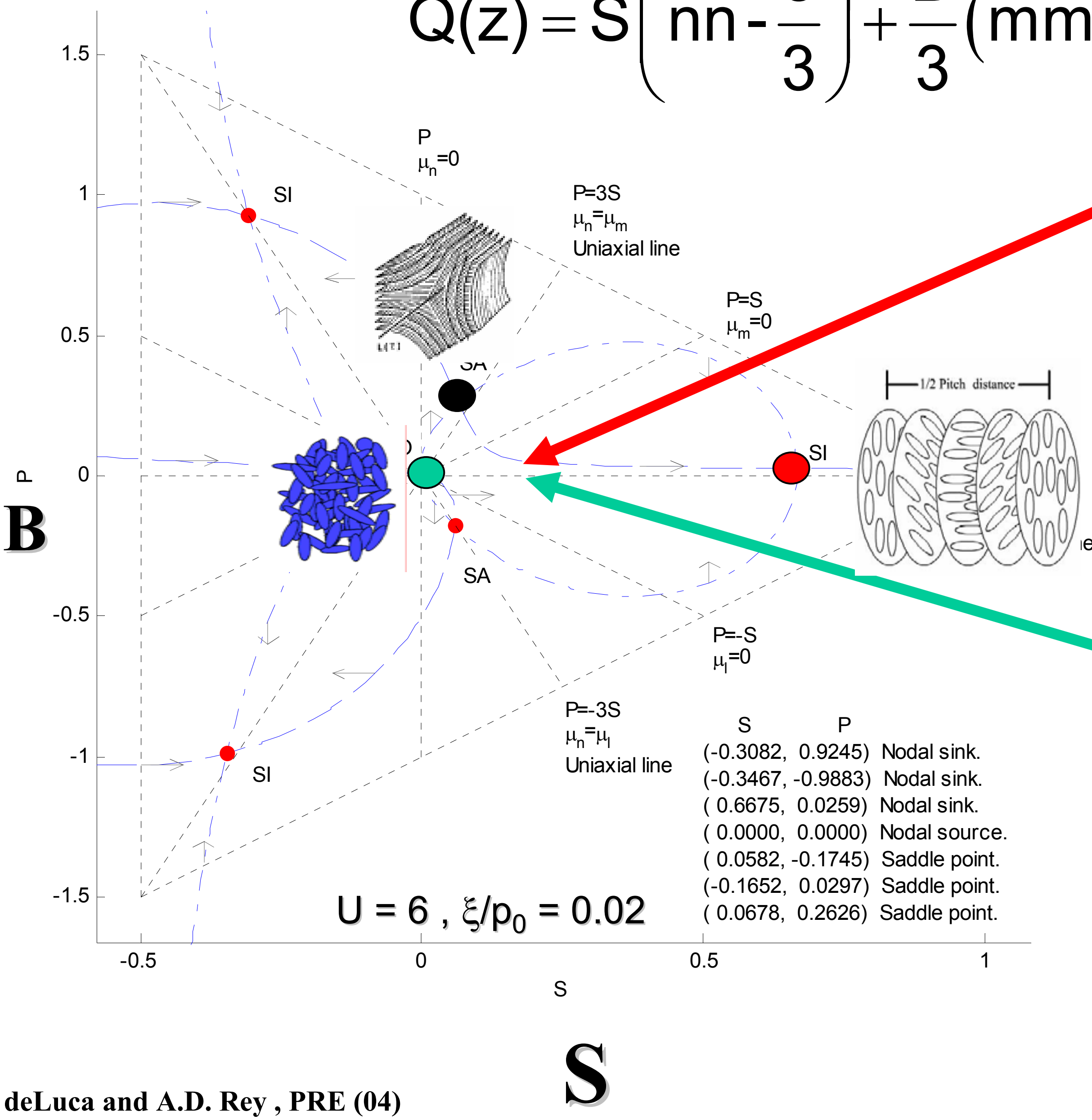

1. Solitons:
SA-SI connections

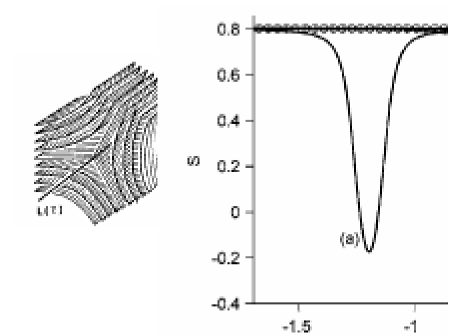

2.Traveling Fronts:
SO-SI connections

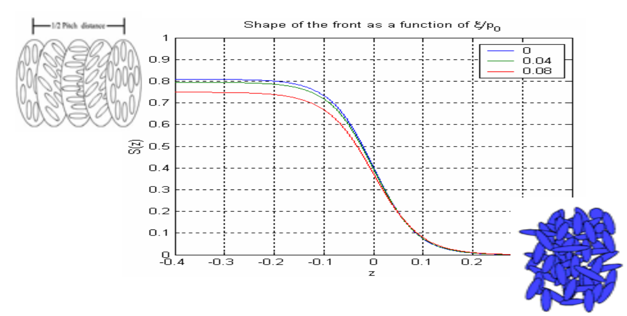

G. deLuca and A.D. Rey , PRE (04)

Chiral Self-Assembly Model

$$\gamma \frac{\partial Q}{\partial t} = -\left[\frac{\partial f}{\partial Q} - \nabla \cdot \frac{\partial f}{\partial \nabla Q}\right]^{[s]}$$

$$-\frac{\partial Q}{\partial t} = \left\{(1-\frac{U}{3})Q - U(Q\cdot Q)^{[s]} + U\,\mathrm{tr}(Q^2)Q\right\}$$

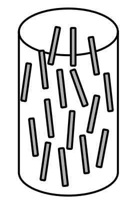

$$-\left(\frac{\xi}{h_0}\right)^2\left(\nabla^2 Q - [\nabla\cdot(\nabla Q)^T]^{[s]} + \upsilon[\nabla(\nabla\cdot Q)]^{[s]}\right)$$

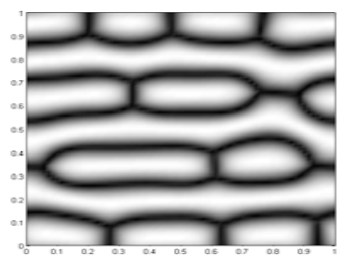

$$\left(\frac{\xi}{h_0}\right)\left(\frac{\xi}{p_0}\right)\left(-8\pi(\nabla\times Q)^{[s]}\right) + \left(\frac{\xi}{p_0}\right)^2\left(-16\pi^2 Q\right)$$

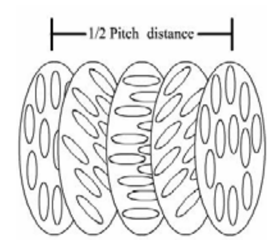

G. deLuca and A.D. Rey , PRE (04)

Nucleation and Growth: Solitons + Traveling Fronts (Hex. Sym)

$$\mathbf{k}_1 + \mathbf{k}_2 + \mathbf{k}_3 = \mathbf{0}$$

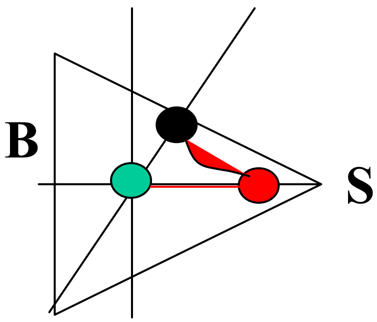

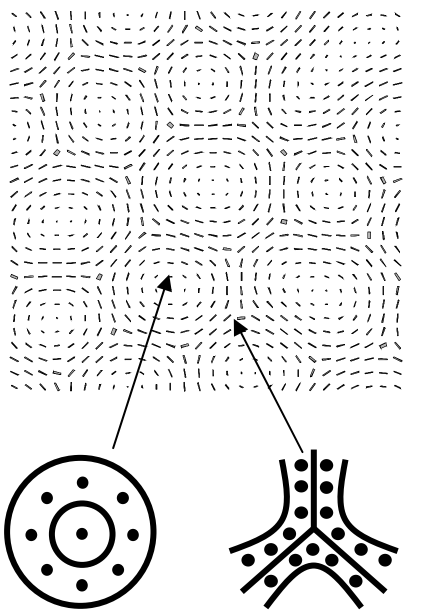

λ2+ τ−

Charge balance: -((6)-2)/2+ 2=0

S = alignment

Red = High Alignment

Blue = Low Alignment

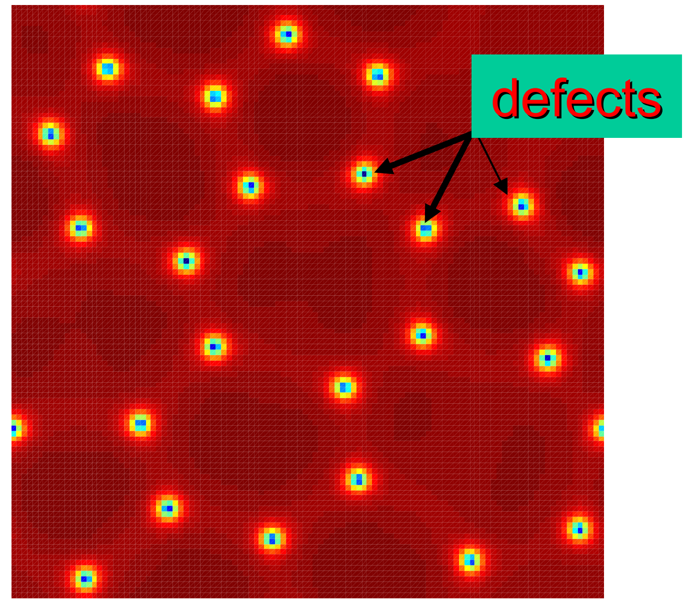

$|n_z|$ = Orientation

Red = Out-of-plane

Blue = In plane

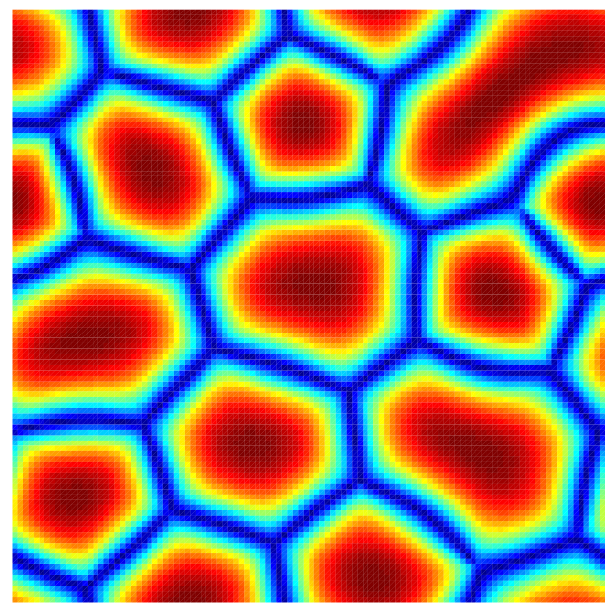

Directed Growth: Unidirectional Traveling Fronts

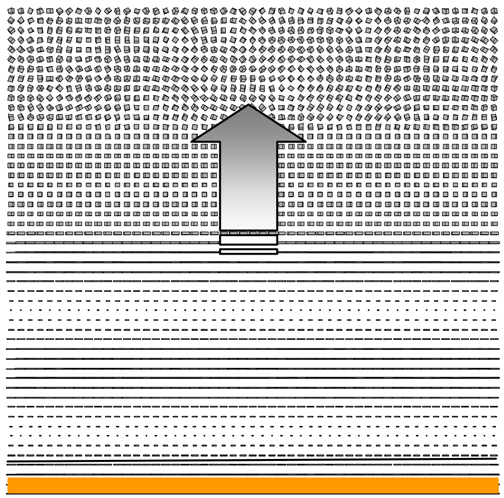

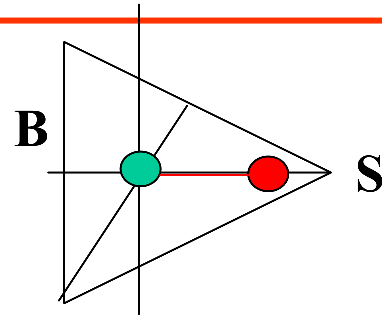

Steady-state

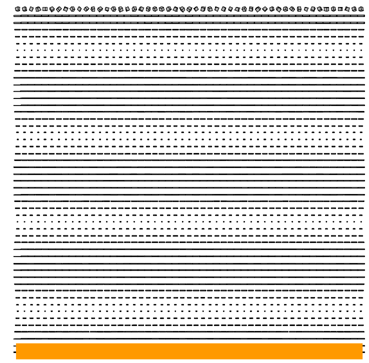

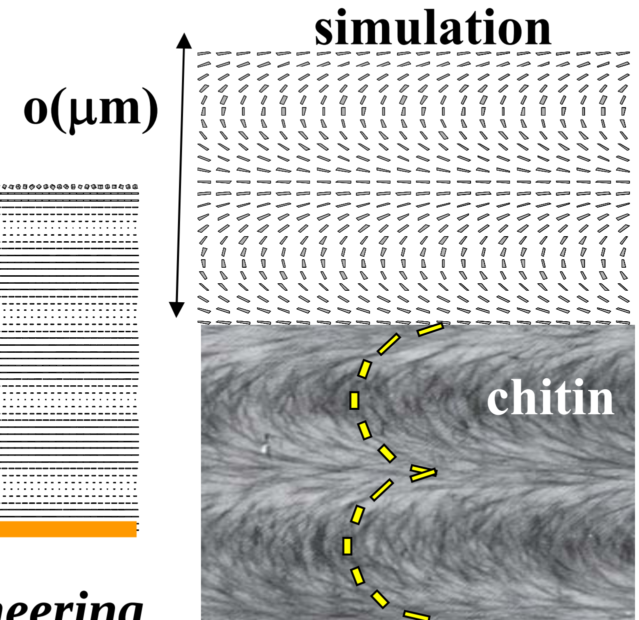

Strong planar anchoring

MAIN DESIGN TOOL:Interfacial Engineering

$$\underbrace{\left.\frac{\partial \tilde{U}^s}{\partial \mathbf{n}}\right|^{[s]}}_{\text{energy}} + \underbrace{W\ \mathbf{kk}}_{\substack{\text{anchoring}\\ \text{tensor}}}\cdot\left\{\underbrace{T\left.\frac{\partial \mathbf{n}^e}{\partial T}\right|}_{\text{entropy}} + \underbrace{\sum_{i=3}^{N}\mu_i^s\left.\frac{\partial \mathbf{n}^e}{\partial \mu_i^s}\right|}_{\text{adsorption}}\right\} = 0$$

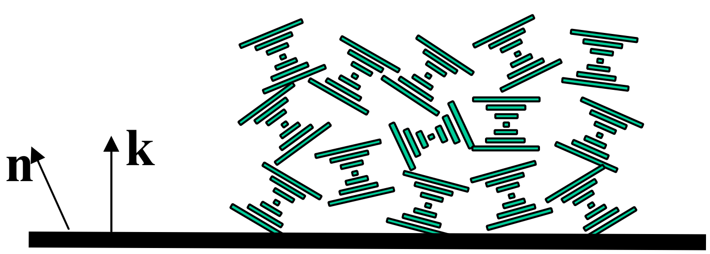

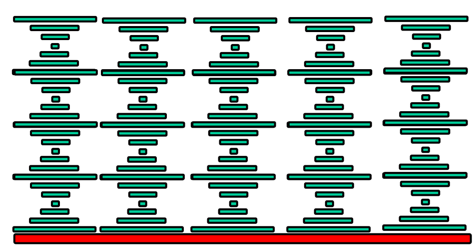

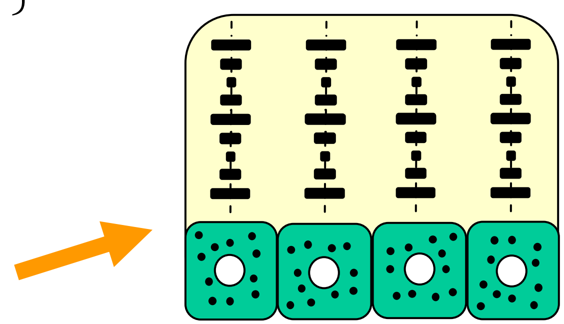

G. deLuca and A.D. Rey , PRE (04) **A.D. Rey, JCP (2003)** **A.C. Neville, "Biology of Fibrous Composites", Cambridge University**

Moving Homogeneous Flat Phase Ordering Fronts

$$f\;/\;ckT=\frac{1}{2}\left(1-\frac{U}{3}\right)\mathrm{tr}(\mathbf{Q}^2)-\frac{U}{3}\mathrm{tr}(\mathbf{Q}^3)+\frac{U}{4}\left[\mathrm{tr}(\mathbf{Q}^2)\right]^2+\frac{\mathrm{L}_1}{2}\nabla\mathbf{Q}\,\vdots\left(\nabla\mathbf{Q}\right)^{\mathrm{T}},$$

$\mathrm{U}=3\mathrm{T}^*/\mathrm{T}$

$$\frac{\partial S}{\partial \mathrm{t}}-\frac{2}{3}\left(\frac{\xi}{\mathrm{h}_0}\right)^2\frac{\partial^2 S}{\partial y^2}=\left(-\frac{2}{3}+\frac{2}{9}U\right)S+\frac{2}{9}US^2-\frac{4}{9}US^3.$$

$$S(\mathrm{y},\mathrm{t})=S(\mathrm{y}-v\mathrm{t})=S(\mathrm{y}');\;\xi=\sqrt{L_1\,/\,ckT}$$

$$v\frac{dS}{dy'}+\underline{\frac{2}{3}\left(\frac{\xi}{\mathrm{h}_0}\right)^2}\frac{d^2S}{dy'^2}-\frac{4\mathrm{U}}{9}(S-S_1)(S-S_2)(S-S_3)=0,$$

$S_1=0$ **isotropic**

$S_2=\frac{1}{4}-\frac{1}{4}\sqrt{9-\frac{24}{U}}$ **max energy**

$S_3=\frac{1}{4}+\frac{1}{4}\sqrt{9-\frac{24}{U}}.$ **nematic**

$$S(y-Vt)=\frac{S_3}{2}\left\{1-\tanh\left[K\frac{S_3}{2}(y-Vt)\right]\right\}\quad K=\sqrt{\frac{U}{3}}\left(\frac{\xi}{\mathrm{h}_0}\right)^{-1}$$

Front Velocity

$$V=\frac{2}{3}\sqrt{\frac{U}{3}}\left(\frac{\xi}{\mathrm{h}_0}\right)\left[-\frac{1}{4}+\frac{3}{4}\sqrt{9-\frac{24}{U}}\right]$$

V>0: *U* > *Uc=2.7* stable N → I

V<0: *U* < *Uc=2.7* stable I → N phase

V=0 :*U* = *Uc=2.7* the interface becomes static

Front Velocity: 0.1m/sec

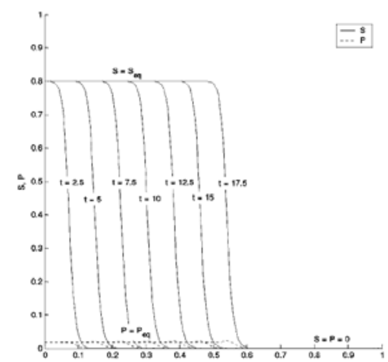

Popa-Nita and T.J. Sluckin, J. Phys. II**(1996).**

Process Kinetics: Speed of Chiral Fronts

$$v = \sqrt{\frac{U}{3}\left(\frac{\xi}{h_0}\right)}\left[-\frac{1}{4}+\frac{3}{4}\sqrt{9-\frac{24}{U}-\frac{96}{U}\pi^2\left(\frac{\xi}{p_0}\right)^2}\right]$$

$$V_{achiral} > V_{chiral}$$

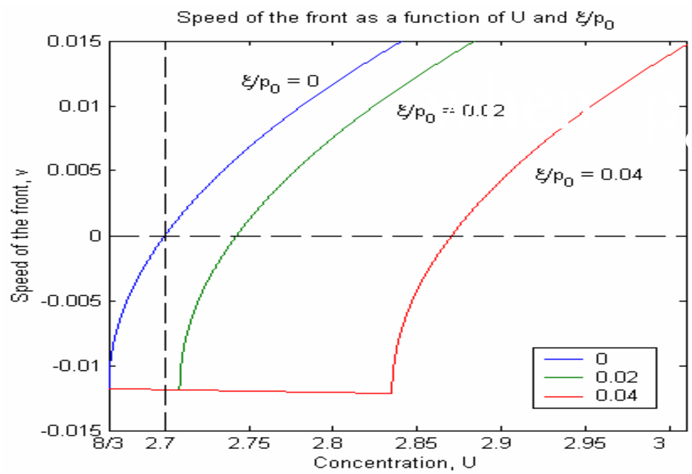

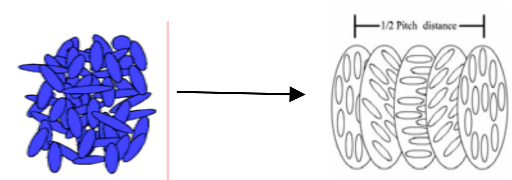

Moulting Process

$$Velocity \approx \xi \times D_r \propto \frac{1}{L^7}$$

"The shell can take between a few hours and a few weeks to fully harden, depending on species. They do this by absorbing calcium carbonate whilst the chitin hardens."

Intact molted shell of an American lobster.

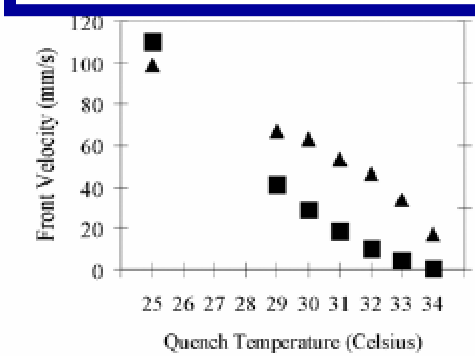

G. deLuca and A.D. Rey , PRE (04), B. Wincure and A.D. Rey, JCP (2006)

Spider Silk Spinning

"Nature uses Liquid Crystal Self-Assembly to produce Super-fibers"

Main Issue: use modeling to discover spider biospinning principles of value to super-fiber manufacturing.

Motivation: Super-fiber Manufacturing

Spinning of synthetic fibres

$T = 300\ ^{o}C$

H_2SO_4

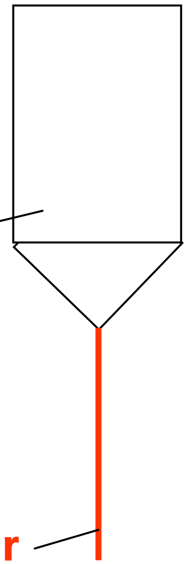

Kevlar

Liquid Crystalline Solution

Material Science

Mechanical Property	Kevlar	Silk
Strength (Nm^{-2})	$4x10^9$	$1x10^9$
Elasticity (%)	5	35

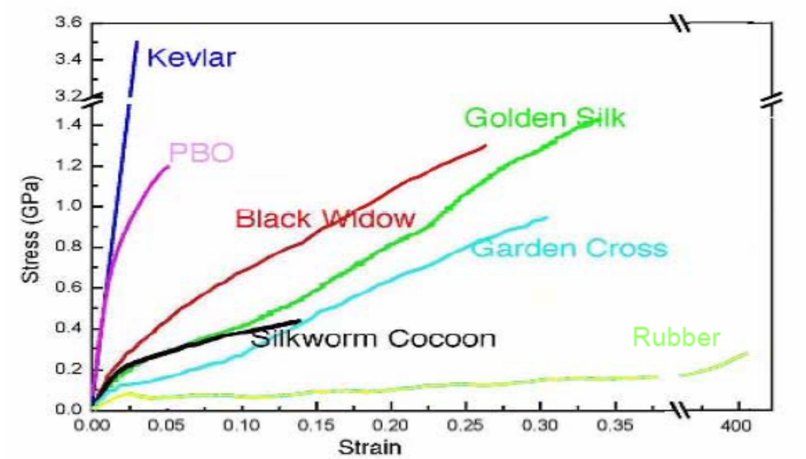

Spinning of natural silk

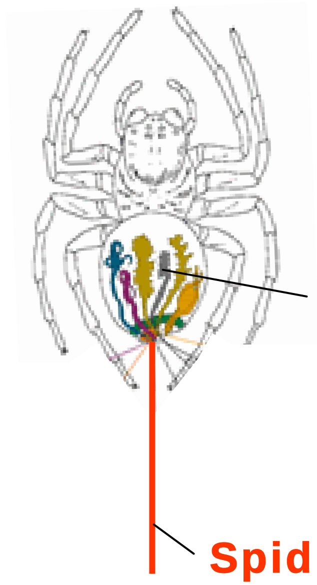

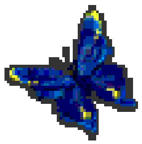

$T = 20\ ^{o}C$

$P = 1\ atm$

H_2O

Spider's silk

Liquid Crystalline Solution

From J.M. Gosline, Endeavor, 1986

Spider Silk Fiber Biospinning Process

Table 1. ^{13}C labeling percentages of silk samples from *N. edulis*

AA	DOQSY, 1-^{13}C Ala, %	DOQSY, 1-^{13}C Gly, %	DECODER, 1-^{13}C Ala, %	DECODER, 1-^{13}C Gly, %	Relative abundance of amino acids,* %
Ala	27.2 (17)	10.0 (7)	11.8 (6)	10.1 (24)	29
Gly	3.9 (10)	59.4 (2)	1.9 (6)	48.1 (23)	40
Pro	1.9 (1)	1.6 (8)	1.6 (6)	1.4 (4)	3
Tyr	−1.1 (23)	−1.0 (25)	−1.0 (19)	1.5 (5)	4
Glu	4.0 (9)	3.5 (2)	1.9 (3)	2.9 (4)	10

The absolute labeling degree of the five most abundant amino acids in silk is given in percentage, together with the relative abundance of the respective amino acids in molar percentage. The title of each column refers to the experiment and the intended labeling. SDs are given in brackets.

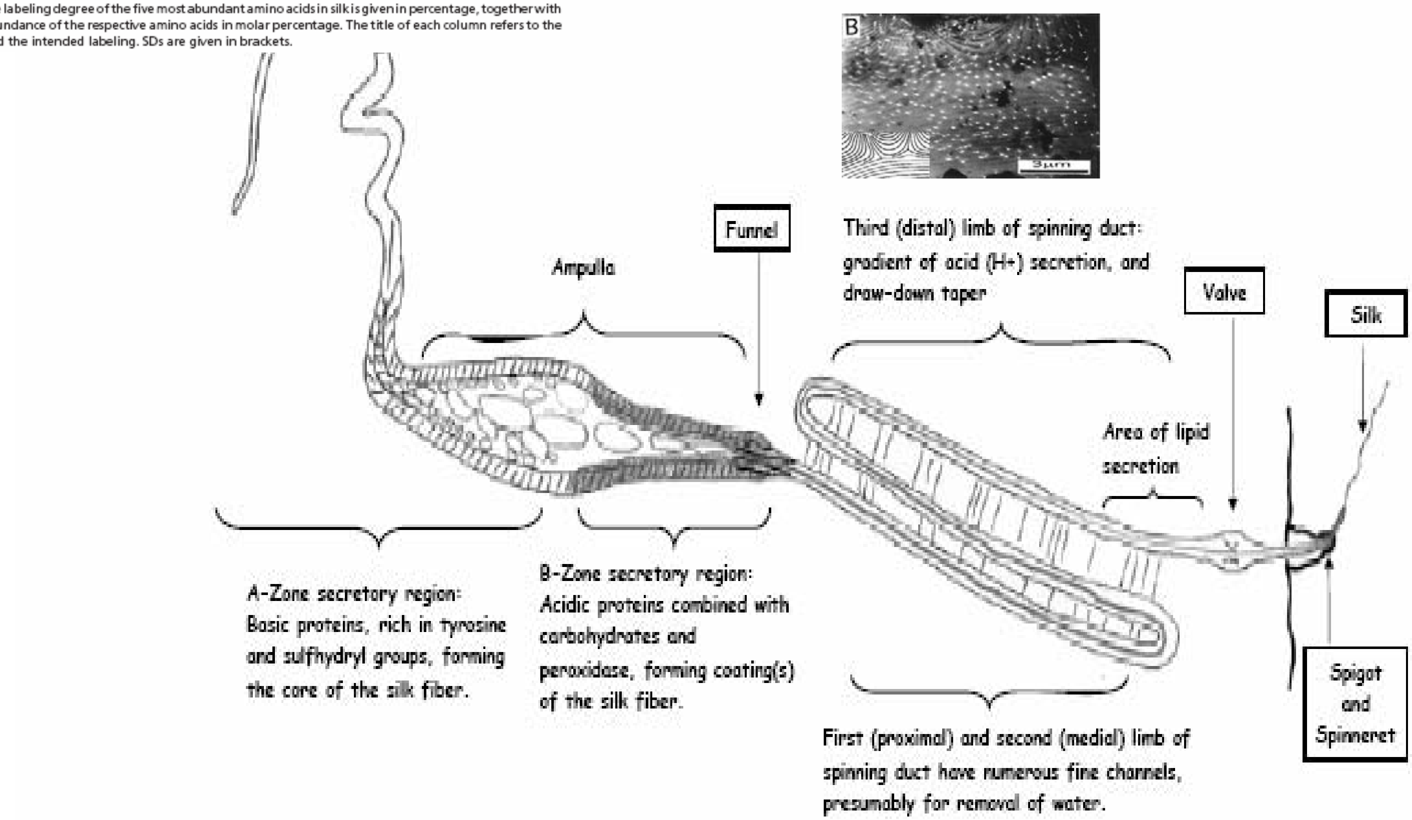

β-sheets crystals

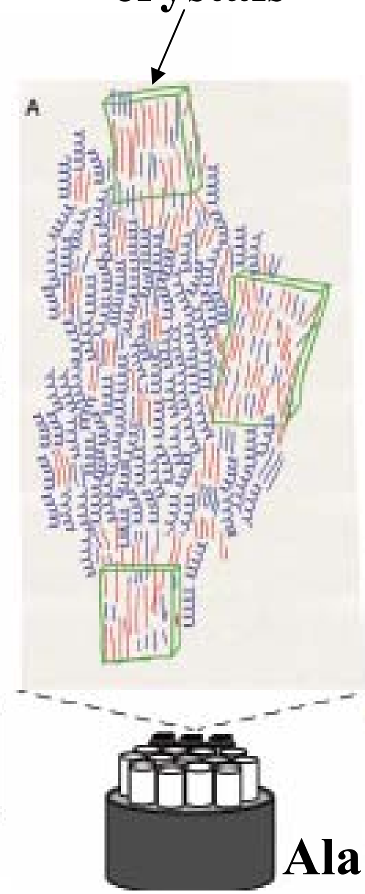

Ala

Gly

1.synthesis 2.self-assembly 3.flow-process 4. solidification

R.F. Foelix, Biology of Spiders, Oxford University Press, J.D. van Beek et al , PNS (2002)

2. Silk Liquid Crystal Self-Assembly

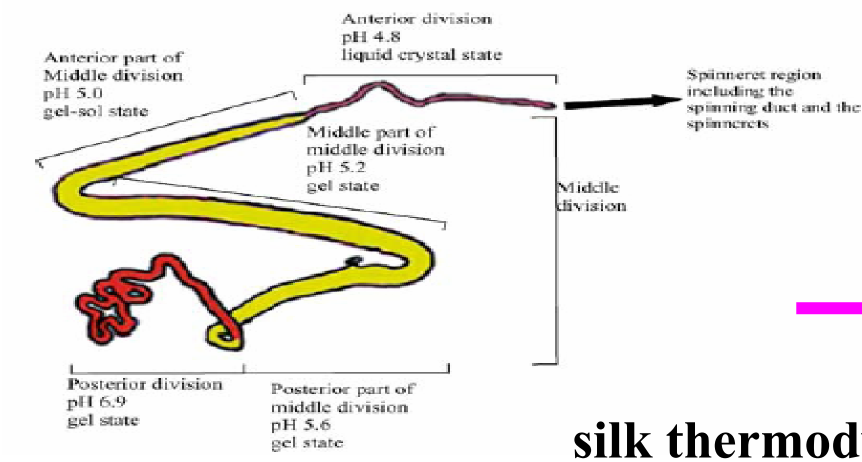

Silk gland	Posterior division	Middle division Posterior	Middle division Middle	Middle division Anterior	Anterior division
pH	6.9	5.6	5.2	5.0	4.8
viscosity	middle	high	high	high	low
state	gel	gel	gel	gel-soln	liquid crystal
K^+ (10^{-3}%)	–	30.2	29.5	33.3	–
Ca^{2+} (10^{-3}%)	–	17.7	46.0	59.7	–
water content (%)	88	75	74	74	70

silk thermodynamics (in progress)

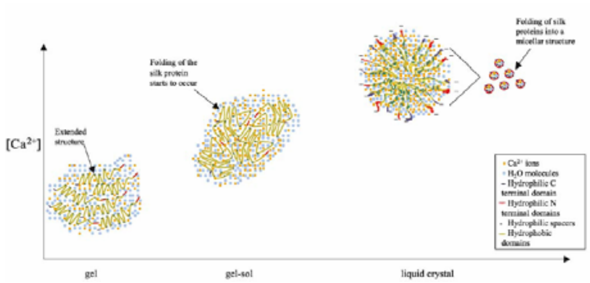

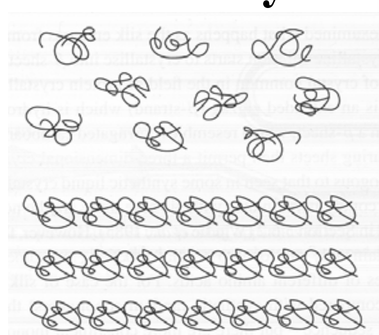

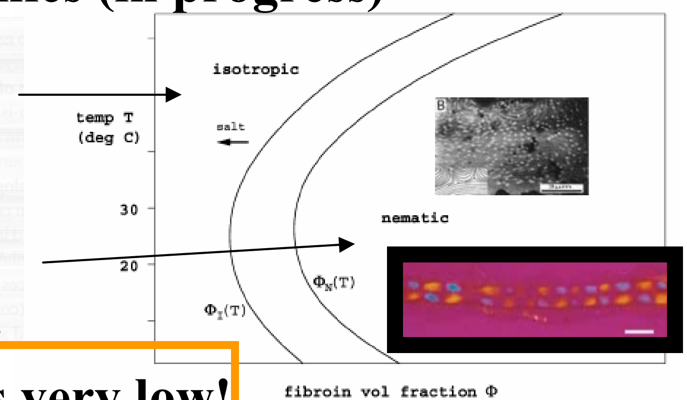

Key Design Principle: LC viscosity is very low!

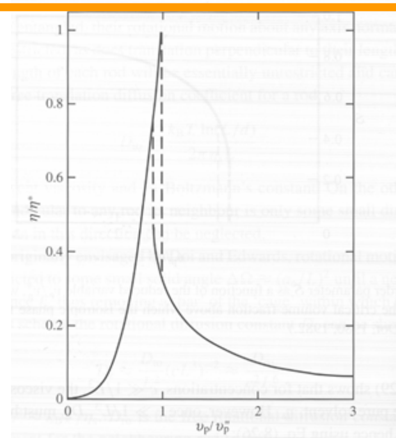

$$\eta = \eta_o\left(1 + nL^3\right)$$

$$\eta = \eta_o\left(1 + 3nD^2L\right)$$

3. Geometry and Flow-Induced Structural Transformations

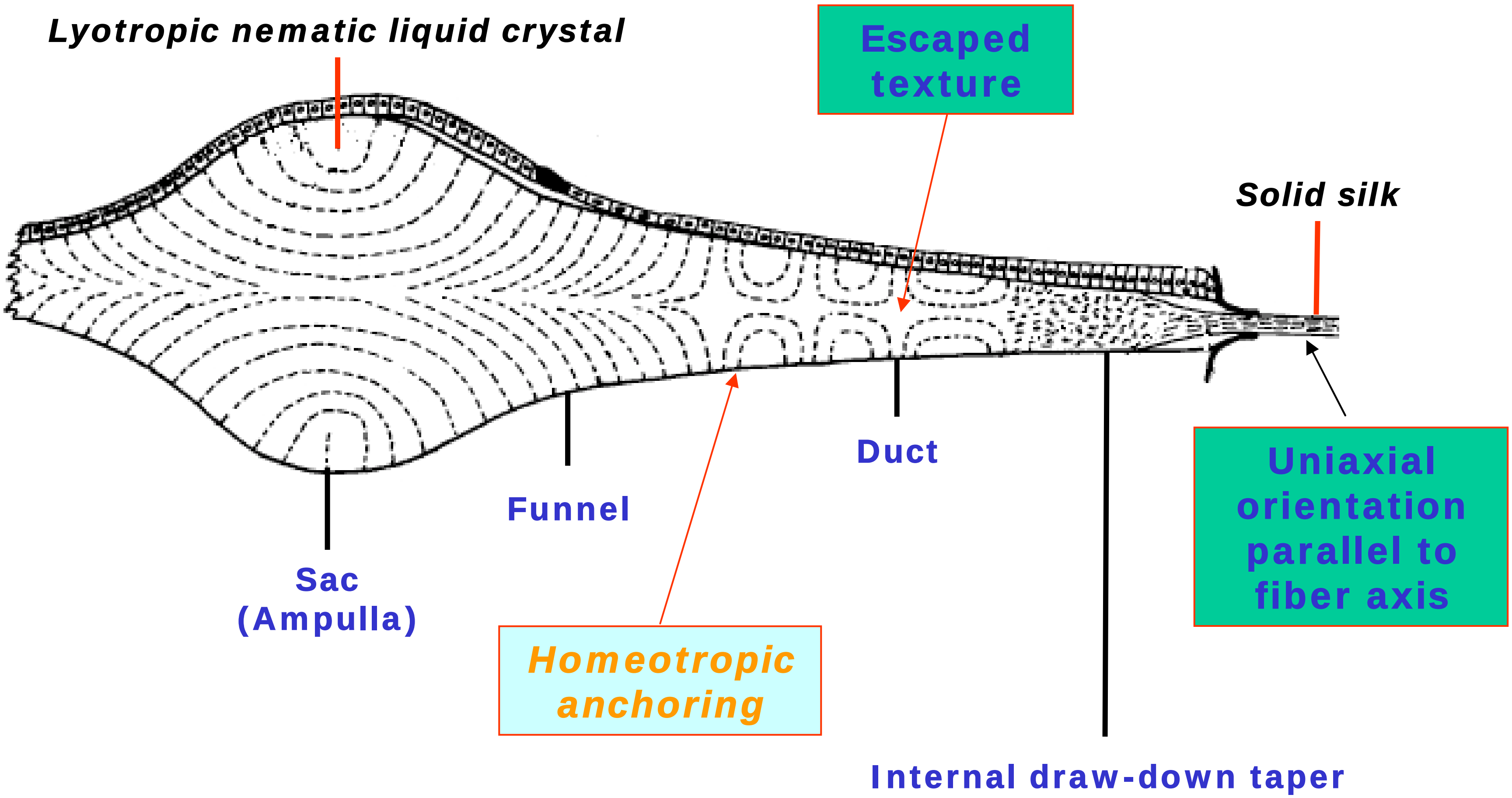

D.P. Knight & F. Vollrath, Proc. R. Soc. Lond. B (1999) 266, 519-523

Facts on Texture in the S-shaped Duct

periodic orientation texture

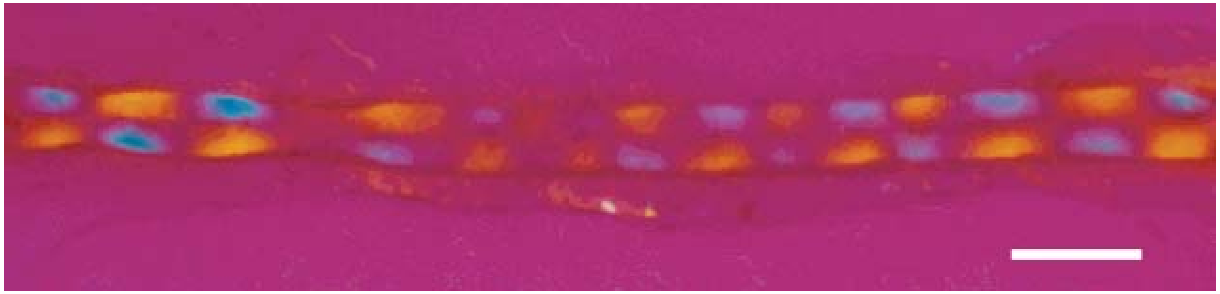

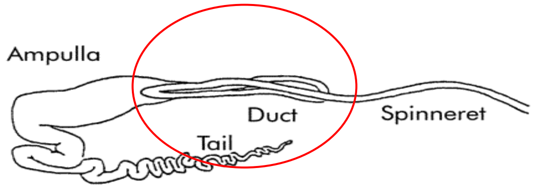

Knight and Vollrath, Biomacromolecules, 2(2), 2001

Polarized Optical Micrograph

Mean repeated period of the pattern ~ 100μm

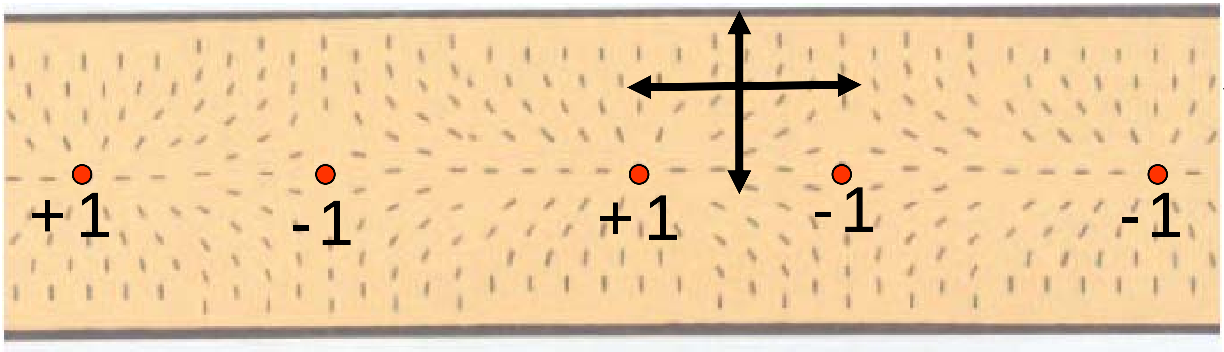

J.E. Lydon, Liquid Crystals Today, 2004, 13(3), 1–13

“Bidirectional Escaped” texture

Peridoc set of hyperbolic and radial nematic point defects

Biospinning Model

$$\frac{\delta \mathbf{Q}}{\delta t} = \beta \mathbf{C}(\mathbf{Q}) : \mathbf{A} - \frac{\mathbf{R}}{\mathbf{E}} \mathbf{f}(\mathbf{U},\mathbf{Q}) + \frac{\mathbf{1}}{\mathbf{E}} \mathbf{f}\left(\nabla^2 \mathbf{Q}\right), \quad \nabla \cdot \mathbf{v} = 0, \quad \nabla \cdot \mathbf{T} = 0$$

$$\mathrm{R} = \left(\frac{\mathrm{H}}{\xi}\right)^2, \quad \mathbf{E} = \dot{\gamma}\boldsymbol{\tau}_n, \quad U = \frac{C}{C^*}$$

DATA

Circular capillary

L=40mm

$20\mu m < H < 100\mu m$

$rate = 10mm/\sec$

$d_f = 4\mu m$

$M_w \approx .5 \times 10^6$

$C = 25\%$

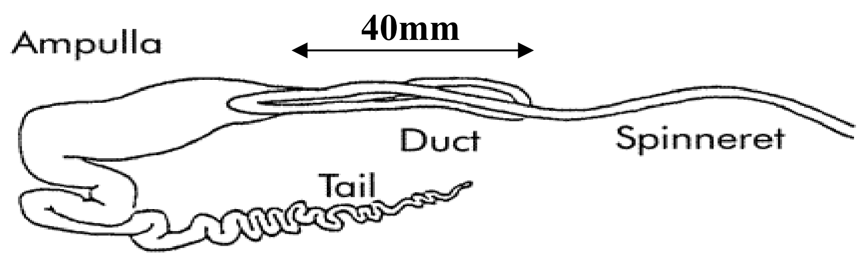

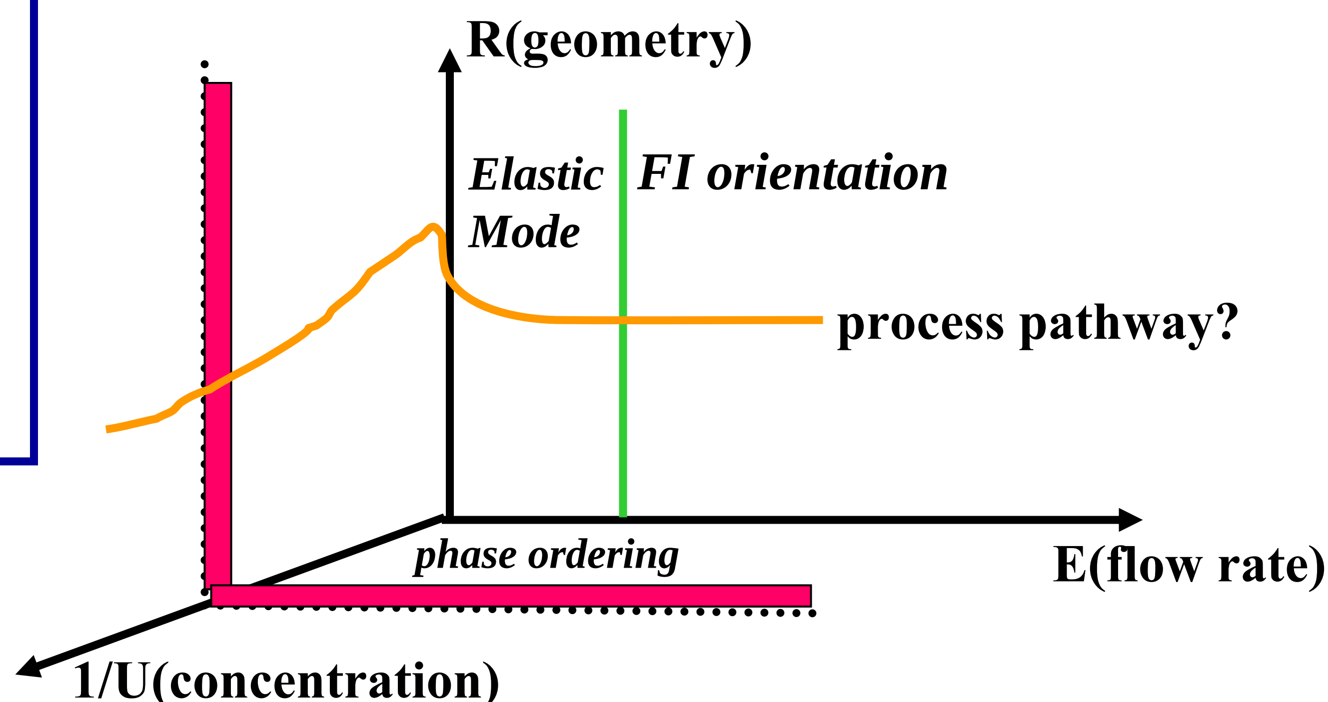

T. Tsuji and A.D. Rey, MTS (1997)

Spider Duct 3D Nematodynamics: Elastic Mode

Bi-directional Escape Texture Formation

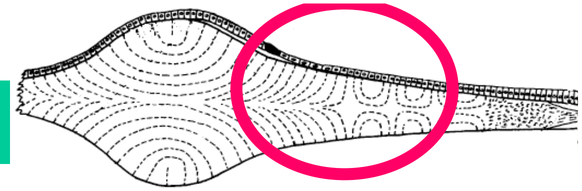

simulations **Spider**

perpendicular anchoring

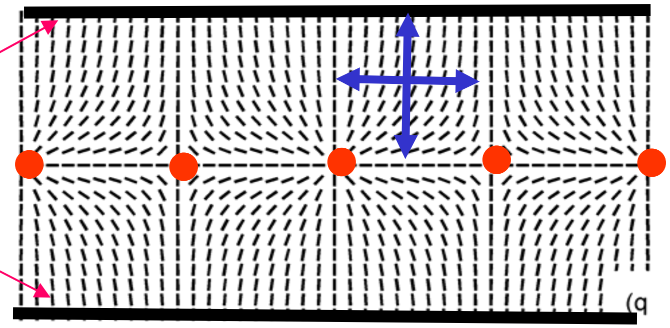

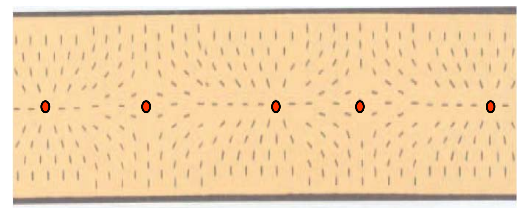

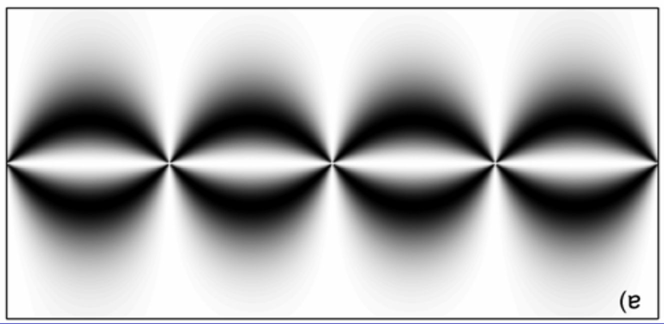

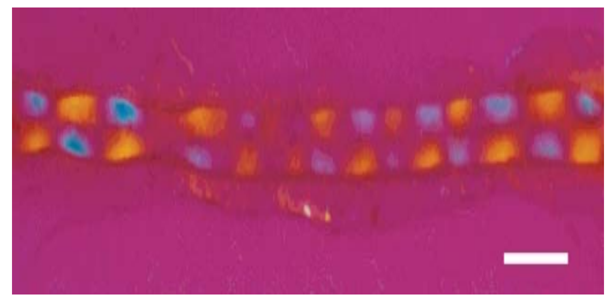

Texture through Interfacial Engineering: Anchoring on Curved Interface

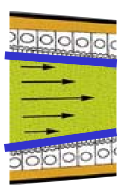

$$\underbrace{\left.\frac{\partial \tilde{U}^{s}}{\partial \mathbf{n}}\right|^{[s]}}_{\text{energy}} + \underbrace{W\ \mathbf{kk}}_{\substack{\text{anchoring}\\ \text{tensor}}} \cdot \left\{ \underbrace{T \left.\frac{\partial \mathbf{n}^{e}}{\partial T}\right|}_{\text{entropy}} + \underbrace{\sum_{i=3}^{N} \mu_i^{s} \left.\frac{\partial \mathbf{n}^{e}}{\partial \mu_i^{s}}\right|}_{\text{adsorption}} \right\} = 0$$

Knight and Vollrath, Biomacromolecules, 2, 2001 **J.E. Lydon, Liquid Crystals Today, 2004, 13** **de Luca and A.D. Rey, JCP (2006)**

On-going work:

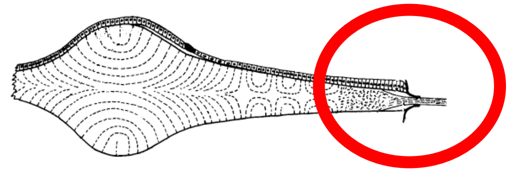

I. Flow-Induced Orientation -Spinneret Nematodynamics

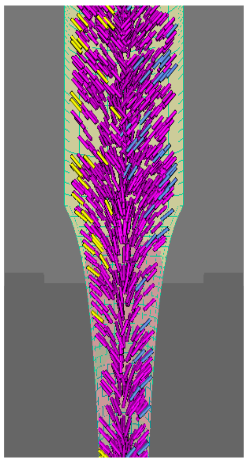

Flow in hyperbolic die

$$A=\begin{pmatrix} pf & sf & sf \\ sf & pf & sf \\ sf & sf & pf \end{pmatrix} \longrightarrow T_{ij}=\eta_{ijkl}:A_{lk} \longrightarrow$$

S=0.9

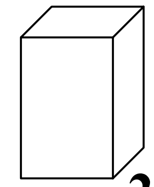

Cry=12%

II. Gel-Crystal Transition

Mw=300,000

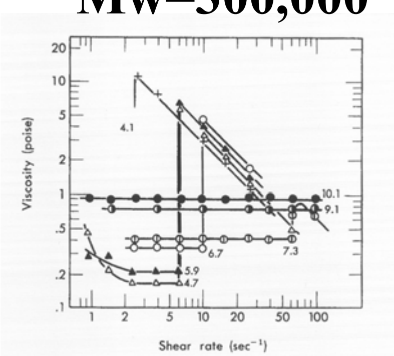

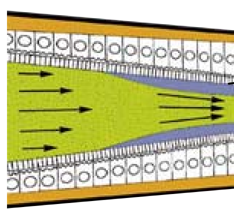

H_20

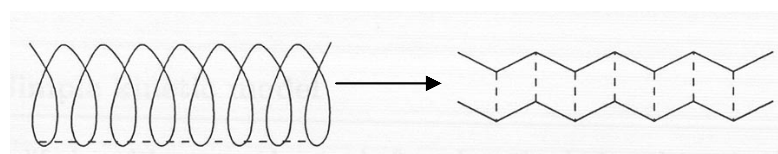

α-helix **β-sheets**

$$Thread\ Stress = mg/Ac$$
$$= .002g/\pi 10^{-10} = 6x10^{7}\ N/m^{2}$$

$$H-H\ Bond\ = 10kJ/mol \times N \times Volume$$
$$= 5x10^{7}\ N/m^{2}$$

E.Iizuka, Adv.Biophys., 24 (1988).

Conclusions

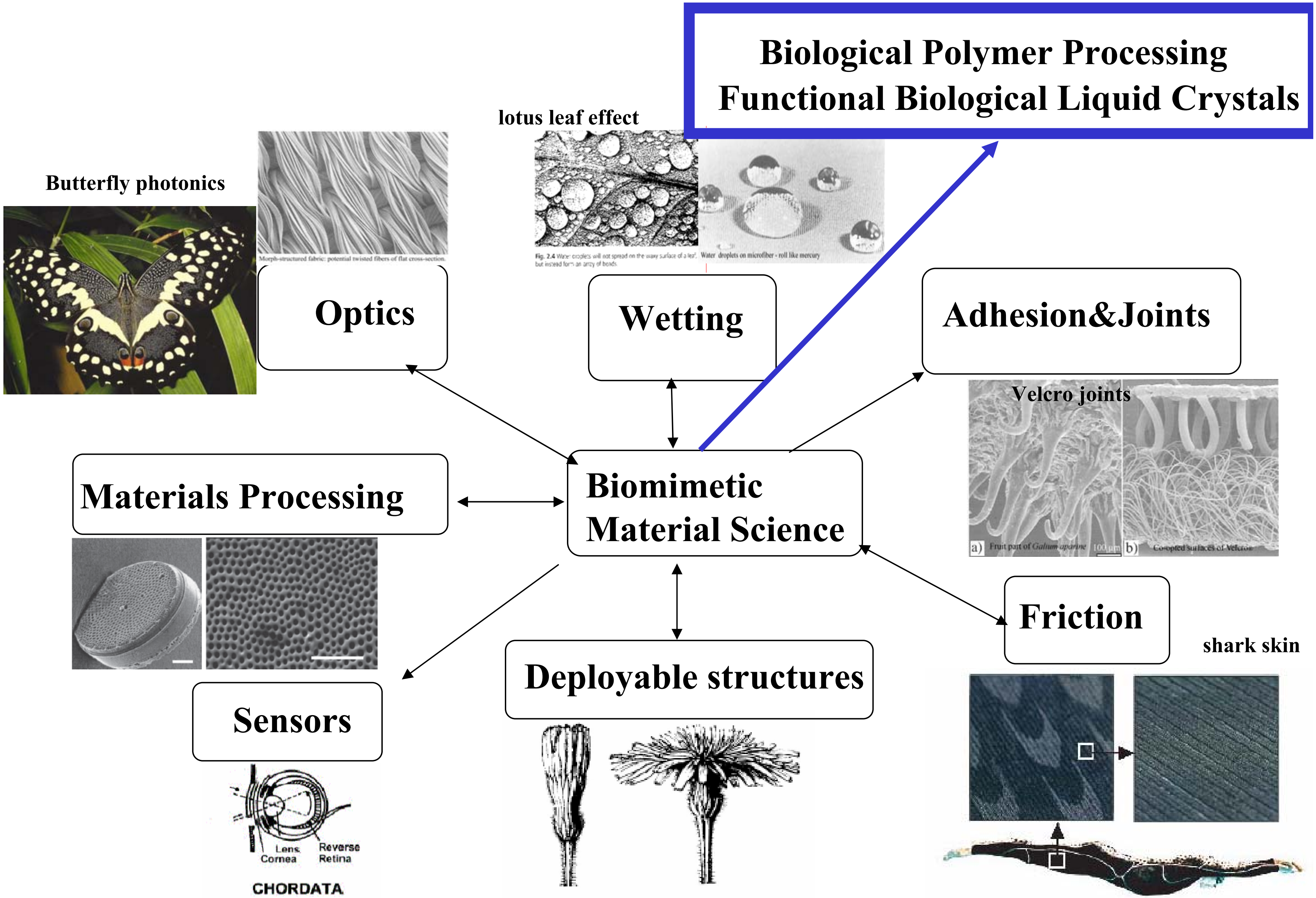

Students and Collaborators

1. Biocomposites

Gino de Luca (McGill), Prof. S. Cowie (CCNY), Prof. D. Passini (McGill)

2. Spider Silk

PhD McGill students:Gino de Luca , N. Abukhdeir
Clemson University Biomimetics Center:
Prof. Chris Cox (Math), Prof. Bert Abbot (Genetics), Michael Ellison (Material Science)

3. Liquid Crystal Self-Assembly

Professor Daniel Lhuiller (P.et M. Curie Institute, Paris)

4. Biomimetics

Professor C. Brebbia, Wessex Institute, UK

Funding: ERC/Center for Advanced Fibers and Films/Clemson University, Natural Science and Research Council of Canada